Arrester-Current Based On-Line MOSA Condition Assessment Using A New Approach

by

Chandana Karawita

A Thesis

Submitted to the Faculty of Graduate Studies

In Partial Fulfillment of the Requirements

For the Degree of

Master of Science

The Department of Electrical and Computer Engineering

The University of Manitoba

Winnipeg, Manitoba, Canada

0-494-08877-X

Library and Archives Canada

Published Heritage Branch

395 Wellington Street
Ottawa ON K1A 0N4
Canada

Bibliothèque et Archives Canada

Direction du Patrimoine de l'édition

395, rue Wellington
Ottawa ON K1A 0N4
Canada

Your file *Votre référence*
ISBN:
Our file *Notre reference*
ISBN:

THE UNIVERSITY OF MANITOBA

FACULTY OF GRADUATE STUDIES

*****

COPYRIGHT PERMISSION

"Arrester-Current Based On-Line MOSA Condition Assessment Using a New Approach"

BY

Chandana Karawita

A Thesis/Practicum submitted to the Faculty of Graduate Studies of The University of Manitoba in partial fulfillment of the requirement of the degree

Of

MASTER OF SCIENCE

To my loving parents

Acknowledgements

I would like to express my sincere thanks to Prof. M.R. Raghuveer for his continuous advice, guidance and encouragement throughout the course of this work. I consider myself privileged to have had the opportunity to work under his guidance. I greatly appreciate the technical support received from Mr. D. Hamelin to carry out my research work. I must also thank Mr. S.N. Fernando, Dr. D. Swatek and Insulation Engineering and Testing Department of Manitoba Hydro for providing us with 36.5 kV station class arresters, which enabled the applicable of the proposed diagnostic techniques.

The financial support received from Manitoba Hydro and the National Science and Engineering Research Council is greatly appreciated. I must also express my gratitude to Mr. W. McDermid of Manitoba Hydro for acting as the liaison officer and project consultant.

I would like to thank Dr.Zeqing Song, all my friends and the staff of the Department of Electrical and Computer Engineering for their continuous encouragement and for making my years at the University of Manitoba a pleasant experience.

This acknowledgement will not be complete without thanking my family. I extend my heartfelt gratitude to my parents. They were always understanding and encouraged me during my hard times. I would like to also thank my sister for all the love and support.

Chandana Karawita

September 2005

Abstract

The degradation of metal oxide surge arresters may be detected by consideration of the resistive component of arrester current. In order to obtain this component, accurate knowledge of the voltage is essential which is difficult in practice. To get around this difficulty a probe-based method was devised in the late eighties and an instrument developed based on that method. In this method the third harmonic component of the resistive current is computed and used as a diagnostic tool. The errors associated with this method have been found to be due to probe positioning and the presence of voltage harmonics.

An alternative and simpler software-based iterative method of obtaining the resistive component has been suggested in literature which relies on the fact that the phase shift between the resistive and capacitive components of arrester current is constant; knowledge of the applied voltage is not required to implement this method. Furthermore, this method does not rely on information gathered from probes and is therefore free of probe related errors. Also, it is claimed that the influence of voltage harmonics is relatively small.

In this thesis, the phase shift criterion has been verified and utilized but in a different manner to obtain the resistive current. The results are compared with the Compensation Technique (Bench Mark Method).

Further more, a new method to assess the condition of MOSA is also proposed in which the fundamental component of the resistive current is used as an indicator. This current is obtained by exploiting the linear relationship, which exists between the peak value of the fundamental component of the resistive current and the phase shift between the fundamental components of the capacitive current and the total arrester current. It is shown that this relationship is independent of temperature, arrester condition and voltage harmonics for a given type of arrester. Results are presented to demonstrate the accuracy and the reliability of the new technique.

List of Symbols

C_p	Inter-granular barrier capacitance
R_p	Inter-granular barrier resistance
r_g	ZnO grain resistance
ω	Angular frequency
G	Capacitive susceptance ($= \omega C_p$)
$[v]$	Applied voltage across the arrester
$[v_{sh}]$	Applied voltage waveform, phase shifted forward by 90^o
$[v_{nsh}]$	n^{th} harmonic component of voltage, phase shifted forward by 90^o
$[i_t], [\overline{I}_t]$	Total arrester current
$[i_c], [\overline{I}_c]$	Capacitive current component
$[i_r], [\overline{I}_r]$	Resistive current component
$[i_{gr}], [\overline{I}_{gr}]$	Generated resistive current component
$[i_{tn}], [\overline{I}_{tn}]$	n^{th} harmonic component total arrester current
$[i_{cn}], [\overline{I}_{cn}]$	n^{th} harmonic component capacitive current
$[i_{rn}], [\overline{I}_{rn}]$	n^{th} harmonic component resistive current
$[I_{r,peak}]$	Peak value of resistive current
$[I_{gr,peak}]$	Peak value of generated resistive current
$[I_{t1,peak}]$	Peak value of fundamental component of total arrester current
$[I_{c1,peak}]$	Peak value of fundamental component of capacitive current
$[I_{r1,peak}]$	Peak value of fundamental component of resistive current
ϕ_{cr}	Phase shift between i_c and i_{gr}
ϕ_{c1t1}	Phase shift between i_{c1} and i_{t1}
$[\Delta I_{gr,peak}]$	Change in peak value of i_{gr}
$[\Delta I_{r1,peak}]$	Change in peak value of i_{r1}
$[\Delta \Phi_{cr}]$	Change in phase shift, Φ_{cr}
$[\Delta \Phi_{c1t1}]$	Change in phase shift, Φ_{c1t1}
k_3/k_1	field factor

Acronyms

ZnO	Zinc Oxide
MOSA	Metal Oxide Surge Arrester
MCOV	Maximum Continuous Operating Voltage
AC	Alternating Current
PC	Personal Computer
THD	Total Harmonic Distortion
FFT	Fast Fourier Transform
RI	Radio Interference
PD	Partial Discharge
EMR	Electro-Magnetic Radiation
A/D	Analog to Digital conversion
CSV	Comma Separated Value file format

Table of Contents

List of Figures

List of Tables

Chapter 1

General Introduction

Metal-Oxide surge arresters (MOSA) have been employed in power systems for the protection of electrical equipment since the early eighties. Their function is to absorb the energy associated with over-voltages and limit their magnitude to a safe and acceptable value across connected electrical equipment.

1.1 Zinc Oxide Valve Elements

A MOSA consists of a suitable number of series-connected valve elements. The basic building block of the valve element is the ZnO grain formed in the sintering process. A micro structural view of a ZnO valve element is shown in Figure 1.1. The grain interior is highly conductive and the near-grain-boundary region is highly resistive [1]. These two regions are separated by a depletion layer. Each grain boundary, which consists of two depletion layers; one on either side. is a nonlinear resistance with a voltage drop of approximately 2.5V at a current density of $1mA/cm^2$ [1]. The voltage across the valve element is equal to the sum of the voltage drops across individual barriers connected in series between the electrodes. The current carrying capability of the element is obtained from the parallel combination of the grain barriers and therefore proportional to the cross section of the element.

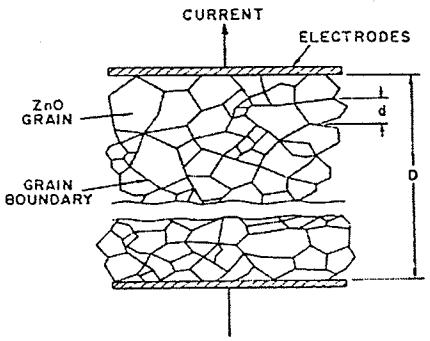

Figure 1.1: Schematic diagram of the microstructure of a ZnO valve element [2]

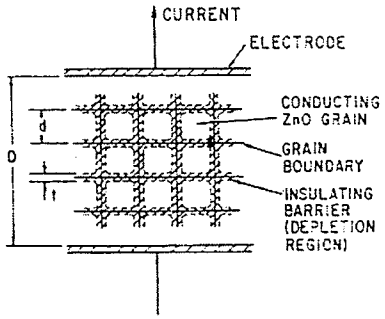

Figure 1.2: Block model of a ZnO valve element [2]

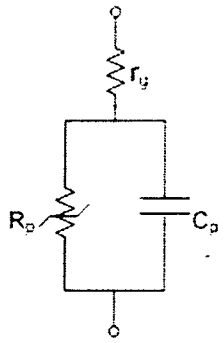

Figure 1.3: Simplified equivalent representation of MOSA [2]

1.1.1 Basic Model

The granular structure of ZnO can be schematically presented by a series and parallel arrangement of the barriers as in Figure 1.2. This block model is used in the analysis of microscopic behavior of ZnO valve elements. The inter-granular barriers are described by an equivalent circuit, shown in Figure 1.3. The parallel combination of capacitor, C_p. and non-linear resistor, R_p, represents the barriers and the small resistance, r_g, of the ZnO grains is in series with the parallel combination. Usually, r_g. is ignored except for very high arrester currents. The arrester current is separated into two parts; resistive, i_r. and

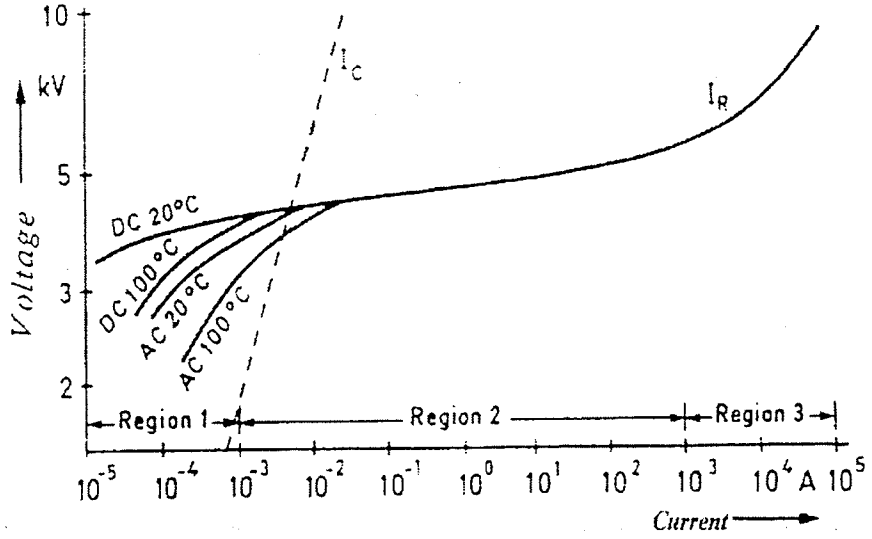

Figure 1.4: Typical V-I characteristics of a ZnO valve element (peak values) [3]

capacitive, i_c, components. The $V - I_r$ characteristics, illustrated in Figure 1.4, shows high nonlinearity due to the behavior of grain barriers. The resistive arrester current may be divided into three regions, i.e. the low electric field region (region 1), medium electric field region (region 2) and high electric field region (region 3).

Under operating voltage, MOSA operates in region 1 and the arrester current is almost capacitive. In this region the conduction mechanism is governed by a forward biased Schottky barrier (thermionic emission) [4] and a very small resistive current flows through the MOSA. The $V - I_r$ characteristics in this region are highly temperature dependent and also depend on frequency. Under transient over-voltage. the MOSA turns on and admits a large resistive current (regions 2 and 3). The voltage across the MOSA does not increase in proportion with the current and therefore apparatus connected across the MOSA is protected. In region 3, the $V - I_r$ characteristics are wave shape dependent.

1.2 Degradation of MOSA

With the passage of time, in service, MOSA exhibit ageing due to the cumulative effect of discharging impulse currents, uneven heating [5] and internal partial discharges [6]. A leading cause of deterioration is ingress of moisture.

Under impulse current, the current density is large which is accentuated by the nonuniform distribution of transient impulse currents. This leads to thermal stresses and cumulatively deform the Schottky barriers. Due to internal partial discharges, Some gases may be generated inside the MOSA housing. These unstable gas molecules react chemically with ZnO granular layers and the electrical properties of the MOSA may deteriorate [5]. Uneven heating also degrades MOSA. This in turn causes nonuniform arrester current distribution and hence, aging.

As mentioned above, The degradation of MOSA is due to the deformation of Schottky barriers in bulk ZnO material [4]. This changes the dielectric properties and hence, the capacitance. The increase in the dielectric loss in low electric field region is also consistent with the deformation of the Schottky barriers. The resistance of the barriers decreases. This can be observed from the change in $V - I_r$ curve due to aging at the low electric field region.

Therefore, ageing manifests itself as an increased component of resistive leakage current [7, 8], accompanying increased power loss and decreased energy absorption capability which in turn may lead to thermal runaway [9]. In spite of all of the above factors it is known that metal oxide surge arresters have been functioning well. However, as their end of life approaches experience has shown that it is desirable to periodically conduct diagnostic tests.

1.3 Diagnosis of Degradation of MOSA

Over the years, although several diagnostic methods [10] based on measurement of radio interference (RI), partial discharges (PD) and emitted electromagnetic radiation (EMR) have been suggested, those based on the measurement of arrester current have offered the

most promise.

In the arrester current based techniques, the arrester current is measured and the resistive current component, which can be used as a diagnostic indicator is estimated by modeling MOSA as a nonlinear resistor in parallel with a capacitor. If the measured waveform of the applied voltage is available, a compensation technique can be used to derive the resistive current. Although this is the most desirable method to check the condition of MOSA, it is not suitable for on-line applications since knowledge of applied voltage is required.

A popular on-line diagnostic procedure involves determination of the third harmonic content of the arrester current. This method gained popularity because it does not involve measurement of the voltage. Recognizing that the third harmonic component so determined also contains a capacitive component arising due to the presence of voltage harmonics, researchers developed a probe-based method [13] to account for the latter component. The resistive third harmonic current is derived for diagnostic purpose. This method however is not free of error as has been demonstrated in [11, 12]. There is an inherent error associated with this method due to the fact that the magnitude and phase angle of harmonic voltages influence the third harmonic component of the resistive current. Operator error is also present which arises because of probe placement. Moreover, use of an approximated field factor introduces an additional error.

Perhaps the best diagnostic method is one that relies on examination of the resistive volt-ampere characteristic. However, in an on-line situation one can obtain the resistive component only at the operating voltage. In [15], a method is suggested to obtain the resistive current from the measured total arrester current without resorting to measurement of the voltage. The resistive component is derived, based on consideration of the current waveform characteristics. This method has been further discussed and analyzed in this thesis.

In this research work, existing arrester current based diagnostic procedures were first analyzed. The motivation behind analyzing these techniques was to design a proper diagnostic

procedure to determine the degradation of MOSA on-line.

1.4 Research Objectives and Achievements

The main objectives of this research were to review the available arrester-current based diagnostic methods and identify the problems associated with them. In particular, the thesis considers the method outlined in [15] and offers a clearly delineated diagnostic technique based on the suggested criteria in that publication.

Furthermore, a new arrester current based diagnostic technique, which has on-line applicability, has been proposed and developed. The influence of voltage harmonics and valve element temperature on the proposed methods has been examined. The Compensation Technique (Bench Mark Method) has been used to validate the proposed methods.

1.5 Thesis Overview

The thesis progressively discusses the approach employed to achieve the above targets.

Chapter 2 gives a brief overview of the existing arrester current based diagnostic procedures. More emphasis was placed on two popular diagnostic techniques,i.e. the Compensation Technique and the Probe Based Method. Their advantages and disadvantages are discussed in brief.

The suggested arrester current wave shape based method is considered in Chapter 3, in a manner different from that reported in [15]. The diagnostic procedure is clearly explained. The developed procedure was applied on the recorded waveforms of valve elements under different operating conditions as well as actual distribution and station class arresters. The results are compared with that of Compensation Technique. The proposed method was further examined for the influence of voltage harmonics and valve element temperature. The advantages and difficulties associated with this method are discussed in this chapter.

In chapter 4, a new method to assess the condition of Metal-Oxide Surge Arresters is presented in which the fundamental component of the resistive current is used as an indica-

tor. This current is obtained by exploiting the linear relationship, which exists between the peak value of the fundamental component of the resistive current and the phase shift between the fundamental components of the capacitive current and the total arrester current. Results are presented to demonstrate the accuracy and the reliability of the new technique.

Finally, in chapter 5 conclusions are drawn and some suggestions given for future work. The appendices at the end introduce the details related to the main chapters of the thesis. References are made to the appendices wherever required.

Chapter 2

Existing Diagnostic Techniques

Various methods for on-line and off-line diagnostics on MOSA have been proposed in the literature [8, 13, 15]. The main diagnostic techniques, which are applicable in AC systems are selected for comparison.

2.1 Off-Line Diagnostic Techniques

2.1.1 Compensation Technique

This is the most straight forward method to derive the *resistive component* from the total arrester current. The measured waveform of the applied voltage is required to implement this method. This method, which may be used as a bench mark method for the comparison of accuracy of other methods, was originally proposed in [8] and modified in [11, 12] to take voltage harmonics in to account.

The *resistive current component* can be written as in 2.1, if the simplified equivalent circuit of MOSA (Figure 2.1) is used.

$$i_r = i_t - i_c \tag{2.1}$$

Where i_t, i_r and i_c are total arrester current, resistive and capacitive components respectively.

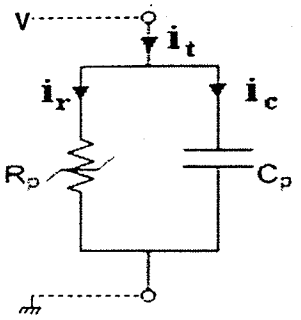

Figure 2.1: Simplified electrical representation of MOSA

If the applied voltage is a pure sine wave, the capacitive current component can be written as shown in 2.2.

$$i_c = Gv_{sh} \tag{2.2}$$

Where v_{sh} is the the applied voltage, phase shifted forward by 90^o and $G = \omega C_p$.

The resistive current is in-phase with the voltage and the capacitive component is orthogonal to the voltage. Therefore, these currents satisfy,

$$\int_0^{2\pi} i_c i_r d\omega t = 0 \tag{2.3}$$

Combining Equations 2.1, 2.2 and 2.3,

$$\int_0^{2\pi} v_{sh}(i_t - Gv_{sh}) d\omega t = 0 \tag{2.4}$$

This is the concept of the Compensation Technique. However, this can not be directly employed in practical cases, since the applied voltage is seldom a pure sine wave. The method was modified in [11] to take voltage harmonics in to account.

According to [11],

$$\int_0^{2\pi} v_{1sh}(i_t - Gv_{1sh}) d\omega t = 0 \tag{2.5}$$

Where v_{1sh} is the the fundamental component of the applied voltage, phase shifted forward by 90^o.

If the measurements of applied voltage and total arrester current are available, the value of G can be numerically determined to satisfy Equation 2.5. Next,

$$i_c = \Sigma n G v_{nsh}, n = 1, 2, 3, ... \tag{2.6}$$

In Equation 2.6, v_{nsh} is the n^{th} harmonic of applied voltage, phase shifted forward by 90^o.

Since the capacitive current is known from 2.6, the *resistive component* can be derived from 2.1, the peak value of which is used as a diagnostic indicator. For an unaged MOSA, this peak value is in the range of $50 - 250\mu A$.

This method relies on availability of the measured voltage waveform. In the field this is difficult and therefore, this method is limited to laboratory diagnostics.

2.1.2 Definition of resistive current and generated resistive current

The *"resistive current"* is defined by,

$$i_r = i_t - \Sigma n G v_{nsh}, n = 1, 2, 3, ... \tag{2.7}$$

In this thesis, the *"generated resistive current"* is defined by,

$$i_{gr} = i_t - G v_{1sh} \tag{2.8}$$

It should be noted that i_{gr} has capacitive harmonic currents embedded in it and that both i_r and i_{gr} are non-sinusoidal even if the voltage is harmonic free. The fundamental components of the *resistive current* and the *generated resistive current* are identical. This component is referred to in this thesis as the *"fundamental resistive current"*.

Figures, 2.2(a) and 2.2(b) show the *resistive current* and the *generated resistive current*

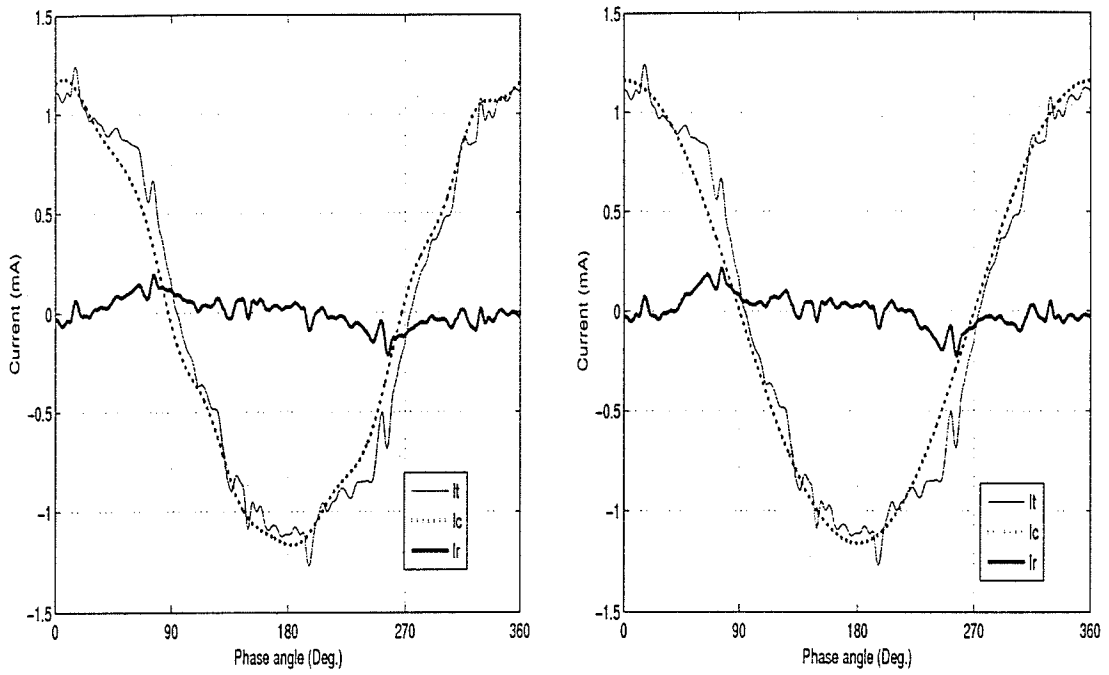

(a) i_{c1} and its harmonics subtracted from i_t (b) Only i_{c1} subtracted from i_t

Figure 2.2: Arrester current components derived by use of Compensation Technique for a ZnO valve element tested at the MCOV

respectively, derived by use of Compensation Technique for a valve element tested at its MCOV. It may be seen that there is not much difference in the peak values of the *resistive* and *generated resistive* currents. This is because the harmonic content of the voltage was small (THD = 1%; 3^{rd}, 5^{th} and 7^{th} harmonics were 0.4%, 0.5% and 0.6% of the fundamental respectively).

2.1.3 Observation of the $V - I_r$ characteristics

Observation of the $V - I_r$ characteristics is one of the best ways to determine the degree of degradation of MOSA. The peak value of the *resistive current* should be derived and tabulated, applying the Compensation Technique, for voltages from about 0.5 MCOV to rated voltage. The voltage versus peak resistive current characteristic is thus obtained. This gives useful information about the condition of the MOSA tested. Figure 2.3 shows how the $V - I_r$ characteristics change when the MOSA is aged. The $V - I_r$ curves of an

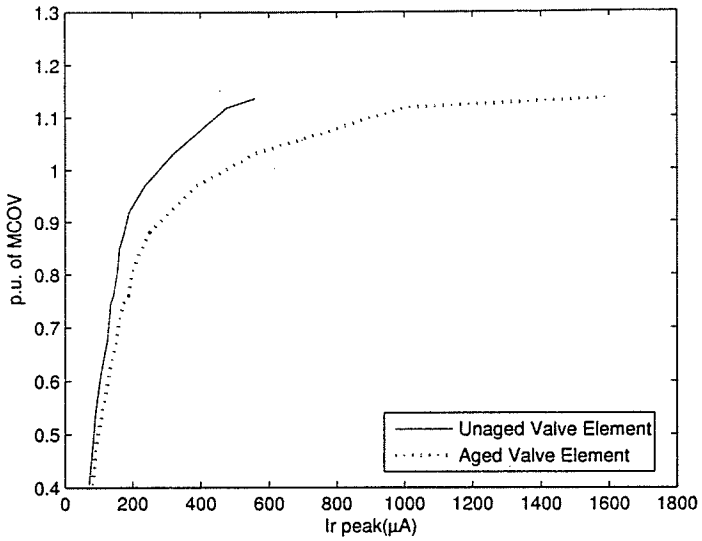

Figure 2.3: $V - I_r$ characteristics of aged and unaged ZnO valve elements

aged and an unaged valve element in the low electric field region are shown.

2.1.4 Measurement of Reference Voltage

The reference voltage is defined as the rms value of voltage applied to the arrester, which results in a peak *resistive current* density of approximately $1\mu A/mm^2$. This definition is not too different from that in IEC 60099-4, which states that "the reference current is the peak value of the *resistive component* of a power frequency current used to determine the reference voltage of the arrester. The typical range is 0.05 mA to 1.0 mA per square centimeter of disc area for single column arresters". The reference current is specified by the manufacturer. It is usually in the range of 1-10mA.

The reference current is obtained at a voltage that is close to the turn on region of MOSA. Therefore, the *resistive component* of the reference current is quite large compared to the capacitive component. As the MOSA degrades the voltage required to obtain the reference current (i.e. reference voltage) changes. The measurement of the reference voltage is used as a figure of degradation.

According to [15], depending on how the reference current is specified in relation to the turn on, the change of the reference voltage caused by the degradation may be positive or negative. Therefore, this is not a reliable indicator[15].

2.1.5 Measurement of Power Loss

The measurement of the power loss is a reliable indicator and gives a picture of thermal properties of the MOSA. Therefore, this method is widely used in laboratories. The power loss is independent of the waveform of the applied voltage and therefore, this method can be utilized for both AC and DC arresters.

2.2 On-Line Diagnostic Techniques

2.2.1 Measurement of Arrester Current

The rms value of arrester current may be measured to evaluate the condition of MOSA. Degradation of MOSA results in an increase in the *resistive current component* and hence the total arrester current.

However, this measurement is not sensitive to a change in the peak value of the *resistive current* because, under nominal applied voltage, the peak value of the capacitive current is in the range of $0.5 - 3mA$, which is much larger than the peak value of *resistive current*, which lies in the range of $50 - 500\mu A$. Therefore, use of the rms value of the arrester current as a diagnostic indicator is not recommended.

2.2.2 Measurement of Neutral Current

This method is only valid for three phase arrester systems shown in Figure 2.4. The zero sequence arrester current is measured at the neutral using a highly sensitive current probe. If the applied voltages are balanced, the capacitive neutral current is zero and the neutral current contains the 3^{rd} harmonic components and its odd multiples of nonlinear resistive currents. Therefore, the neutral current may be used as an indicator.

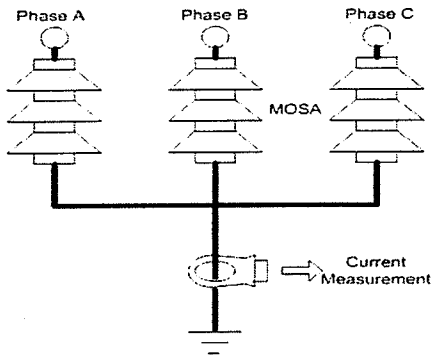

Figure 2.4: Measurement of neutral current

This method however gives an average figure of the conditions of the arresters in the three phase arrangement. The level of degradation of the MOSA in three phases may not be identical and therefore the measurement of the rms value of neutral current is not adequate. The added capacitive current component to the neutral current under unbalanced conditions also causes error in the measurement.

The neutral current method has been modified in [16], based on the wave shape of the neutral current. The neutral current waveform of a three phase arrester system is shown in Figure 2.5. In the neutral current waveform, there is corresponding peak to each phase. According to [16], the corresponding peak will increase as the arrester in that phase ages. In order to identify the phase in which the aged arrester located, total arrester current of one phase is recorded simultaneously with the neutral current. Since the arrester current is almost capacitive in the low electric field region, the peak value of the total arrester current is approximately 90^o ahead of the peak of the applied voltage. By exploiting this fact, the peaks in the neutral current corresponding to each phase can be located. The minimum peak is used as a reference to the others.

According to [16], effect of inter-phase interference and voltage harmonics on the neutral current method is negligible, but unbalanced voltages can introduce errors in the diagnosis provided by the neutral current, which results in incorrect identification of aged MOSA.

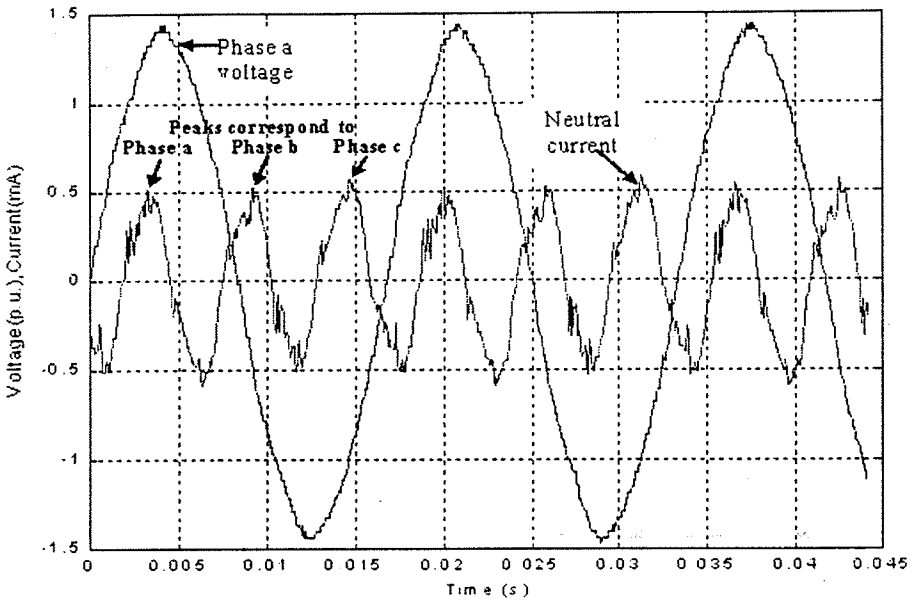

Figure 2.5: Neutral current waveform of a three phase arrester system [16]

2.2.3 Probe Based Method

The nonlinear resistive characteristics of MOSA are responsible for harmonics in the arrester current when the MOSA is energized with nominal sinusoidal voltage. As the arrester degrades the *resistive current* increases and the waveform gets more distorted. The harmonic content, therefore, increases. It is found that the 3^{rd} harmonic content is quite large compared to other higher order harmonics. The 3^{rd} harmonic component under nominal applied voltage increases as the arrester degrades and therefore, the measurement of the 3^{rd} harmonic component may be used for diagnostic purposes.

However, the 3^{rd} harmonic component so determined also contains a capacitive component arising due to the presence of voltage harmonics. Scandinavian researchers [13] developed a probe based method to compensate the added capacitive 3^{rd} harmonic component. An instrument was developed by a Norwegian company, *"TransiNor As"* using the method reported in [13]. A diagram showing the components of the experimental setup is

shown in Figure 2.6.

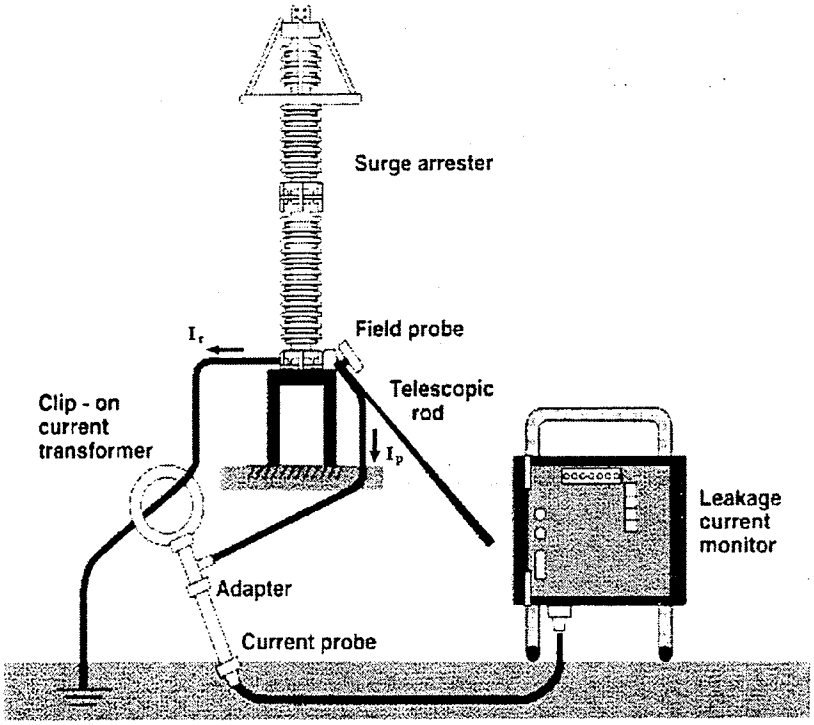

Figure 2.6: Design of the leakage current monitoring equipment Type LCM [14]

Principle of Probe Based Method

A field probe is placed at the bottom of the arrester as illustrated in Figure 2.6. The total arrester current, $\overline{I}_t$, and the probe induced current, $\overline{I}_p$, are recorded. [1]

If the capacitive 3^{rd} harmonic component, $\overline{I}_{c3}$, is subtracted from the 3^{rd} harmonic component of the measured total current, $\overline{I}_{t3}$, the 3^{rd} harmonic resistive component, $\overline{I}_{r3}$, can be obtained as shown in Equation 2.9.

$$\overline{I}_{r3} = \overline{I}_{t3} - \overline{I}_{c3} \tag{2.9}$$

I_{c3} is derived with the aid of the measured probe induced current.

[1] The notations used in section 2.2.3 mirror those used in [13] and are not used elsewhere in this thesis.

According to [13],

$$\overline{I}_{c3} = [\frac{k_3}{k_1}] * [\frac{I_{t1}}{I_{p1}}] * \overline{I}_{p3} \tag{2.10}$$

The field factor, k_3/k_1, depends on the the electric field outside the arrester. For single phase arrangements, this ratio is equal to one, but it is less than one for three phase arrangements due to the influence of other phases on the electric field. In [13], it is claimed that the ratio is approximately 0.75 and therefore, the resistive 3^{rd} harmonic current can be obtained from 2.11.

$$\overline{I}_{r3} = \overline{I}_{t3} - 0.75 * [\frac{I_{t1}}{I_{p1}}] * \overline{I}_{p3} \tag{2.11}$$

Errors in Probe Based Method

The Probe Based Method has been further analyzed in [11]. The following inherent errors have been reported.

- The resistive 3^{rd} harmonic component is not only be influenced by the fundamental and 3^{rd} harmonic voltages, but also by the higher order voltage harmonics such as 5^{th} and 7^{th}. In some practical cases, magnitude of these harmonic voltages may be greater than that of 3^{rd} harmonic voltage. Influence of these harmonics can not be neglected.

- In this method it is assumed that the field factor, k_3/k_1, is constant. However, this depends on the electric field pattern and therefore, on the position of the probe. The results will change with the position of probe.

- The resistive 3^{rd} harmonic component is not sensitive to some degradation modes like, aging due to oxygen reduction and moisture ingress [15]. Therefore, the measurement of resistive 3^{rd} harmonic component is not effective for those modes of degradation.

Chapter 3

Arrester Current Wave Shape Based Diagnostic Technique

In recent literature a method has been proposed for MOSA diagnostics, which has on-line applicability. The basis of this method is examined in this chapter and a clearly delineated alternative technique proposed, which employs the same basis.

3.1 Method Outlined in Literature Employing Phase Shift Criterion

In the method suggested in [15], the *generated resistive current* is obtained from the measured arrester current without resorting to voltage measurement. According to [15], the phase shift between the fundamental capacitive and *generated resistive* components of the arrester current is constant and independent of arrester condition and voltage harmonics. This criterion is used to obtain the *generated resistive current.* A description of the method outlined in [15] suggests that this technique involves the following steps.

1. Total arrester current is measured.
2. A virtual sinusoidal signal is generated from the measured current to represent the fundamental capacitive current. No details are given in [15] about how to determine the magnitude of the virtual reference signal.

3. The reference signal is first selected as in-phase with the total arrester current and it is subtracted from the total arrester current to find the *generated resistive current.* The phase shift between the reference signal and the *generated resistive current* is compared with the phase shift criterion.

4. The reference signal is phase shifted forward and the above procedure is repeated until the phase shift criterion is satisfied.

5. The *generated resistive current* is used for diagnostic purposes.

The phase shift has to be defined as the phase difference between peak positions, as shown in Figure 3.1.

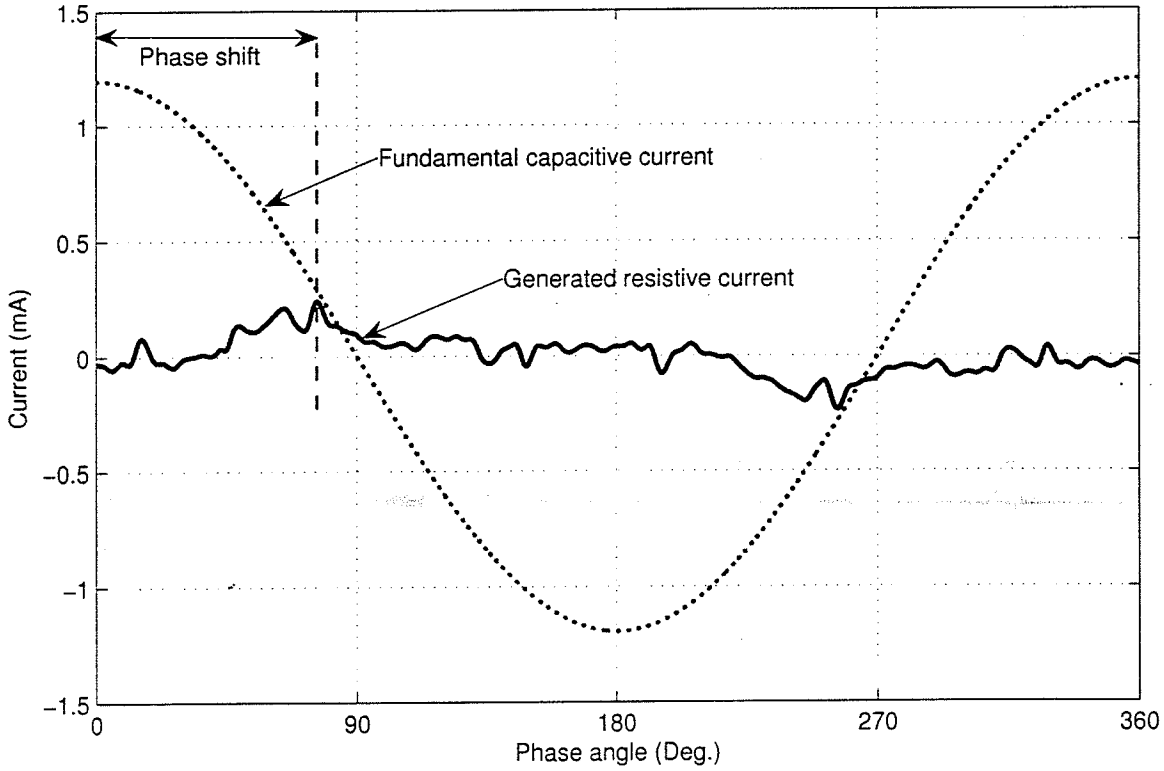

Figure 3.1: Definition of phase shift between the fundamental capacitive and the generated resistive current components

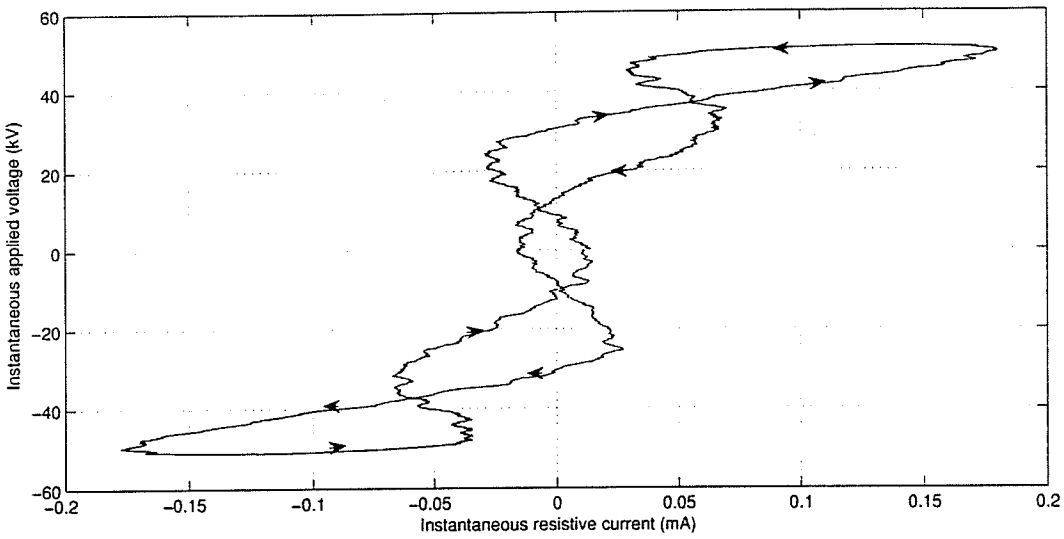

Figure 3.2: Instantaneous $V - I_r$ characteristics of an arrester at its MCOV

In most of the arrester current based diagnostic techniques MOSA is modeled as a nonlinear resistor in parallel with a capacitor. Theoretically, the phase shift between the *resistive* and capacitive current components should be 90^o. In the low current region, where the arrester operates under nominal applied voltage, the *resistive component* shows hysteresis(Figure 3.2) and the phase shift (peak to peak) is less than 90^o [15]. This is illustrated in Figure 3.1.

In this chapter the phase shift criterion suggested in [15] has been experimentally validated. Furthermore a clearly delineated alternative technique has been suggested, which exploits the same criterion.

3.2 Experimental Set-up

3.2.1 Test Specimen

Tests were carried out on the following sets of test objects.

Set-A: One unaged and two aged samples of valve elements, 3" in diameter and 1.75" in height; two in series with selected MCOV of 10kV.

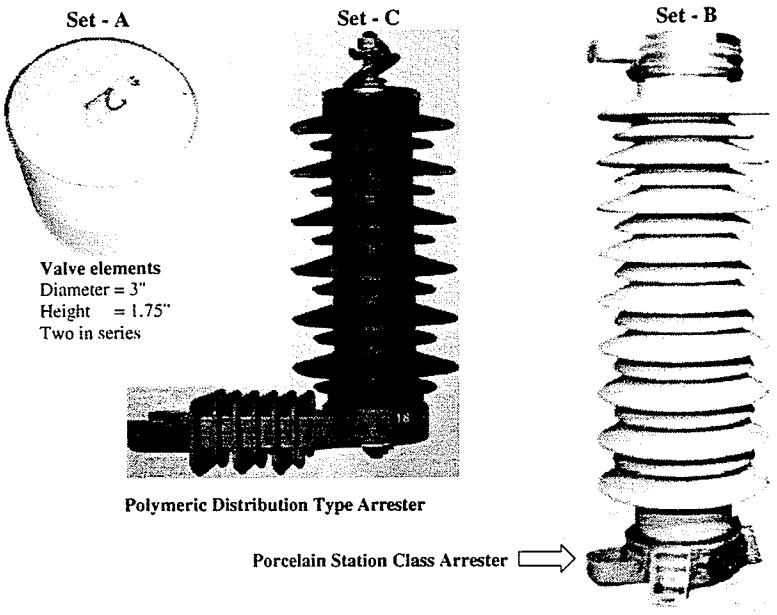

Figure 3.3: Test objects - dimensions are not to scale

The valve elements were tested to obtain $V - I_r$ characteristics and classified as aged if $I_r, peak > 250\mu A$ at MCOV. The aging had been accomplished in earlier work by passage of impulse currents using an impulse current generator [17]. The samples were labeled as unaged, aged-1 and aged-2 according to the following criteria.

- Unaged : $I_{r,peak} < 250\mu A$ at MCOV
- Aged-1 : $I_{r,peak} > 300\mu A$ at MCOV
- Aged-2 : $I_{r,peak} > 500\mu A$ at MCOV

Set-B: 2 no. of new 36.5kV MCOV porcelain station class arresters.

Borrowed from Manitoba Hydro

Manufacturer : General Electric

Set-C: One new 15.3kV MCOV polymeric distribution type arrester

Manufacturer : Joslyn Manufacturing Co.

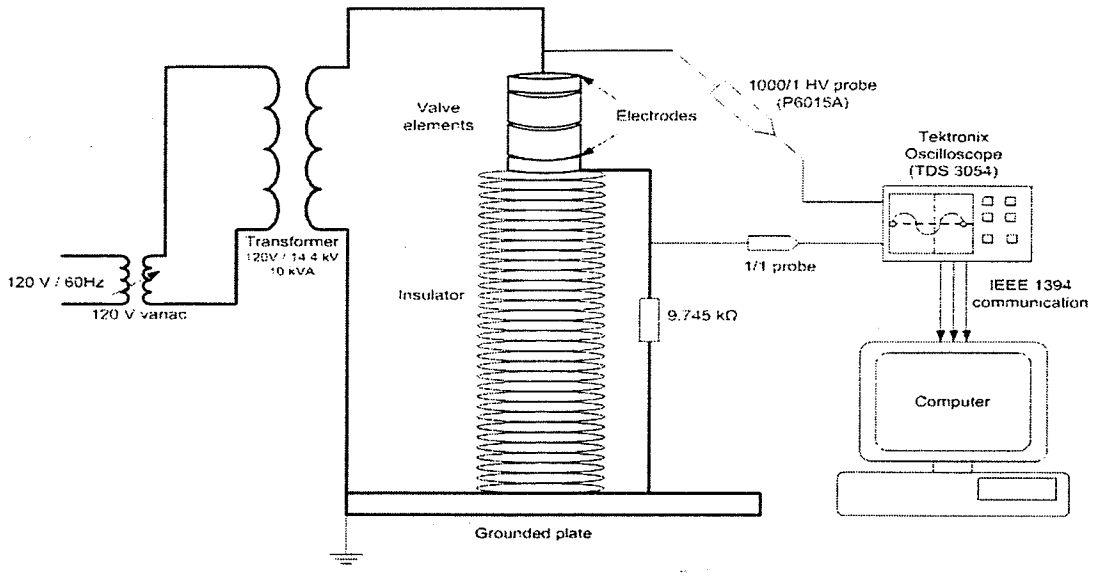

Figure 3.4: Laboratory test setup-1

The test objects are shown in Figure 3.3

3.2.2 Test Set-up

The laboratory test setup shown in Figure 3.4 was used to test MOSA valve elements. While testing the actual arresters, the test setup was modified as shown in Figure 3.5. The transformer was replaced by one with a higher voltage rating and the high voltage probe was replaced by a capacitive voltage divider.

The test objects were tested at different voltages, temperatures and under different voltage harmonic conditions. The waveforms of applied voltage and arrester current were recorded using a Tektronix digital oscilloscope. The recorded waveforms were transferred from the oscilloscope to a PC and then, to a spread sheet by use of WaveStar. A MATLAB program was written to obtain the resistive and capacitive components of the arrester current from the recorded waveforms (Appendix A).

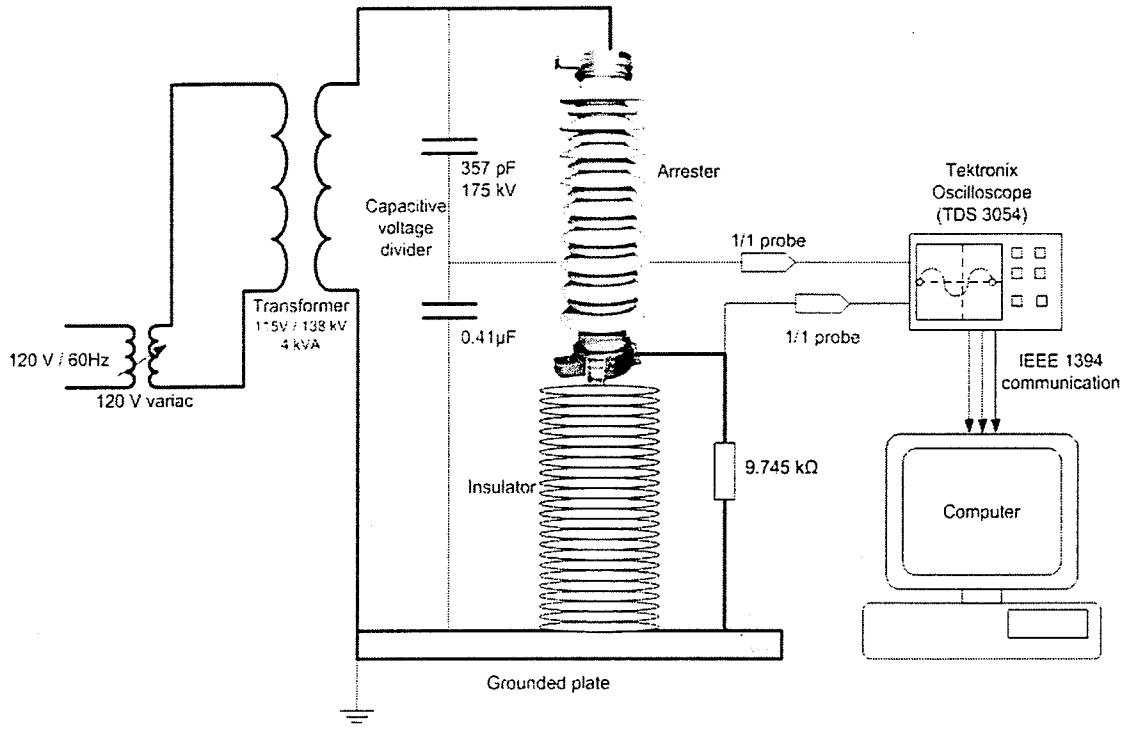

Figure 3.5: Laboratory test setup-2

3.3 Validation of Phase Shift Criterion by Experiment

3.3.1 Effect of temperature, arrester condition and voltage on phase shift criterion

Set-A was first tested at room temperature (23^oC) in the range of voltage of 0.8 - 1.1 pu of MCOV. The phase shift versus voltage characteristics for the three samples at room temperature are shown in Figure 3.6. Next, the valve elements were heated up to a particular temperature in the laboratory oven and the test was carried out in the same range of voltage. The phase shift obtained for Set-A at 23^oC, 50^oC and 70^oC, for four voltages, is tabulated in Table 3.1. The mean value of the phase shift for Set-A is 76.6^o and the standard deviation of the test results is 0.54^o. No significant change in phase shift is observed for the valve elements of different operating temperatures and arrester condition. Small spikes in the recorded arrester current waveform, caused by the operation of micro varistors in the bulk

metal oxide material [15], are responsible for the slight deviations of the phase shift.

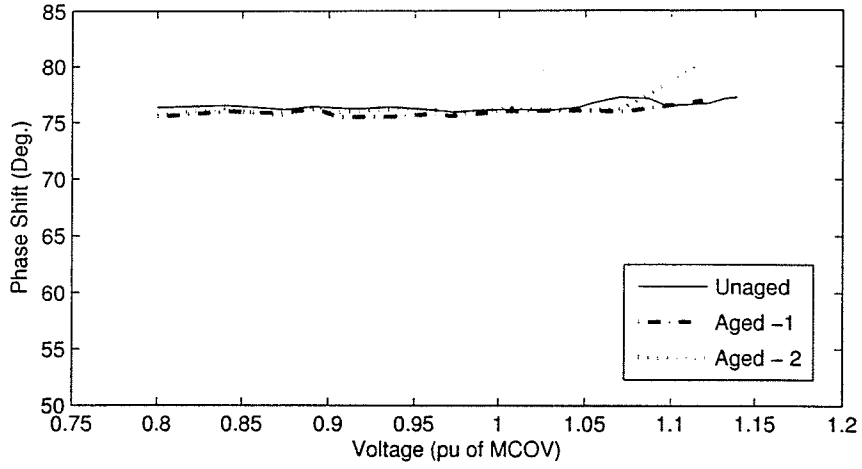

Figure 3.6: Variation of the phase shift criteria with voltage for Set-A at room temperature (23^oC)

Table 3.1: Comparison of Phase shift for Set-A

Voltage pu of MCOV	Sample	Phase shift (Deg.) @ 23 ^oC	Phase shift (Deg.) @ 50 ^oC	Phase shift (Deg.) @ 70 ^oC
0.8	Unaged	76.6	76.5	76.9
	Aged-1	76.0	76.7	77.1
	Aged-2	76.2	76.4	77.7
0.9	Unaged	76.3	76.4	77.2
	Aged-1	75.5	76.6	76.9
	Aged-2	75.9	76.6	77.2
1.0 (MCOV)	Unaged	76.2	76.5	76.9
	Aged-1	75.6	76.7	77.3
	Aged-2	75.9	76.5	77.0
1.1	Unaged	76.4	76.6	77.0
	Aged-1	76.0	76.7	77.5
	Aged-2	76.0	76.8	77.7

Both arresters belonging to Set-B were tested from 0.6 to 1.1 pu of MCOV. The change in the phase shift with applied voltage is depicted in Fig.3.7. A step change in the phase shift was noticed at about 0.85pu of MCOV for both of the arresters in Set-B. This change

is due to the change in the location of dominating spike at the peak of the *resistive current.* Since the arrester is usually operated below 0.8pu of MCOV under normal conditions where the arrester is tested for aging, the phase shift shift criterion is still applicable.

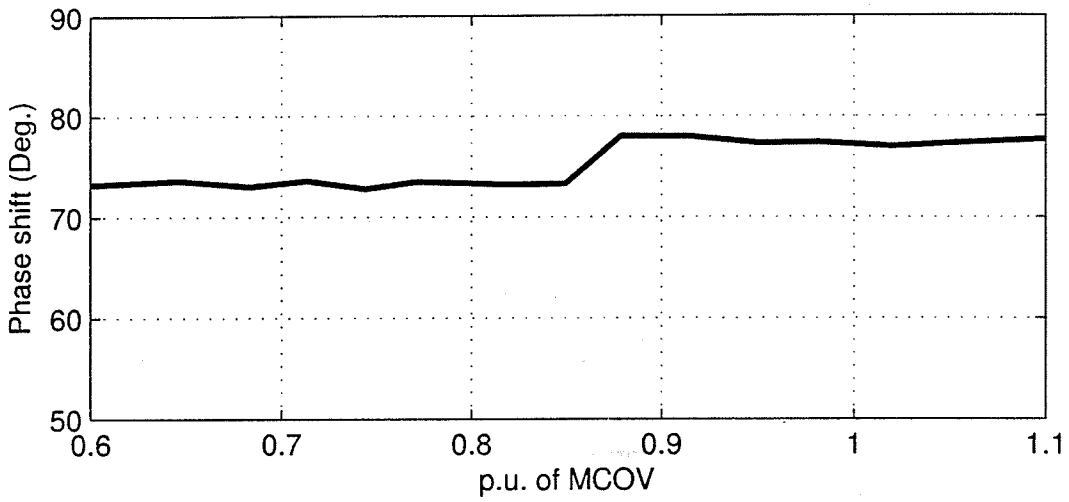

Figure 3.7: Change in phase shift with applied voltage for Set-B

3.3.2 Effect of voltage harmonics on phase shift criterion

In the method suggested in [15], only the fundamental component of the capacitive current is subtracted and all other harmonic capacitive currents are embedded in the *generated resistive current.* In order to find the effect of capacitive current harmonics on the phase shift, Set-C was tested under two different harmonic conditions, i.e, Case 1 and Case 2 in Table 3.2. The results are shown in Table 3.3. It is seen that the phase shift does not change significantly.

Table 3.2: Voltage harmonics

Case	THD	Voltage harmonics		
	(%)	V3 (%)	V5 (%)	V7 (%)
Case 1	1.15	0.31	0.98	0.22
Case 2	0.67	0.59	0.14	0.09

Table 3.3: Effect of voltage harmonics on phase shift

Voltage pu of MCOV	Phase shift (Deg.) Case 1	Phase shift (Deg.) Case2
0.8	77.6	77.5
0.9	78.3	77.0
1.0	78.5	77.8

3.4 Validation of Effect of Voltage Harmonics on Phase Shift Criterion by Simulation

The effect of capacitive current harmonics on the phase shift was further analyzed using numerical simulation. It is known that the 3^{rd}, 5^{th} and 7^{th} capacitive current harmonics are the most significant and the higher order capacitive current harmonics are negligible. The total arrester current of Set-A unaged valve elements at MCOV and 0.8 pu of MCOV were measured and the capacitive harmonic components of the arrester current were obtained using the Modified Compensation Technique. The effect of voltage harmonics was investigated by increasing the magnitudes of the capacitive harmonics as shown in the following cases. The factor "k" represents the magnitude of harmonic components as a percentage of the fundamental capacitive current.

Case A: $modified\ I_{gr} = I_r + k * I_{c3}$; k = 0 to 5% of I_{c1}.

Case B: $modified\ I_{gr} = I_r + k * I_{c5}$; k = 0 to 5% of I_{c1}

Case C: $modified\ I_{gr} = I_r + k * I_{c7}$; k = 0 to 5% of I_{c1}

Case D: $modified\ I_{gr} = I_r + k * (0.5 * I_{c3} + 0.3 * I_{c5} + 0.2 * I_{c7})$; k = 0 to 5% of I_{c1}

The phase shift between the fundamental capacitive current and the modified resistive current was found while the value of "k" increased. The simulation results obtained for the unaged sample of Set-A are illustrated in Figure 3.8. The phase shift is almost constant except for Case C in Figure 3.8(b) where the 7^{th} harmonic capacitive current exceeds 3.6%; but this is rare in practice.

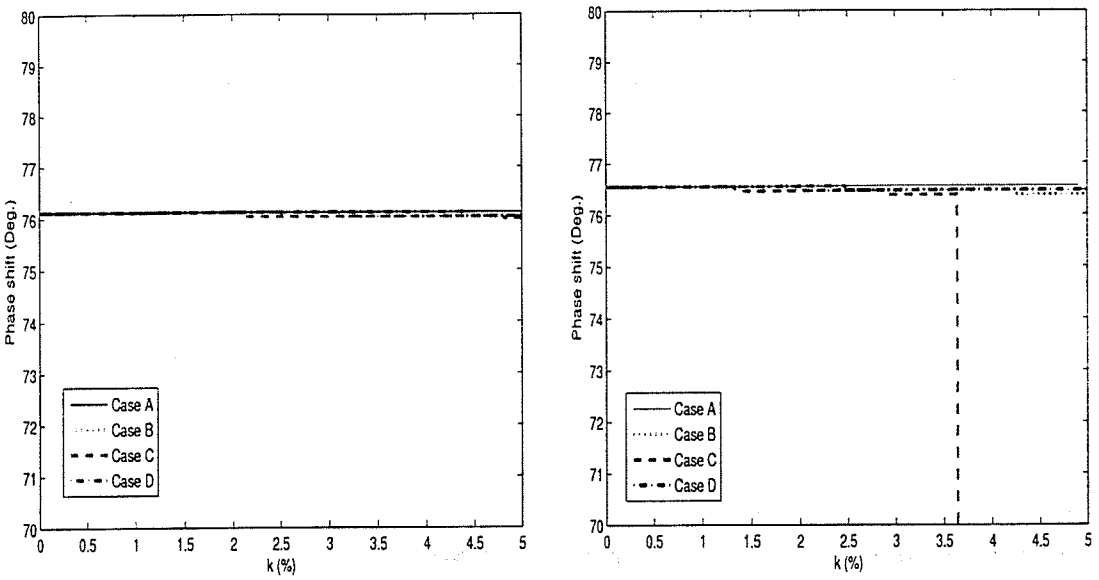

(a) At MCOV (b) At 0.8*MCOV

Figure 3.8: Change in phase shift with capacitive harmonic content -simulation results

Since the *resistive current* is much smaller than the fundamental capacitive current, the capacitive harmonics embedded in the resistive current can not be neglected. However, the simulation results confirm that the effect of capacitive harmonics on the phase shift criterion is negligible.

The above work confirms that the phase shift is almost constant within operating voltage range and the deviation is within two degrees. The phase shift is independent of the arrester condition. The effect of voltage harmonics and temperature on the phase shift is negligible. The claims made in [15] are therefore valid.

3.5 Alternative On-Line Diagnostic Technique Based on Phase Shift Criterion

3.5.1 Description of alternative diagnostic method

The following alternative technique is suggested by the author of this thesis by exploiting the fact that the phase shift between the fundamental capacitive current and the *generated*

resistive current is constant [15].

First, an average value for the phase shift is determined through laboratory experiments. Only the arrester current needs to be recorded on-line and the phase shift criterion is combined with the fundamental principles as follows.

The fundamental component of the recorded arrester current, I_{t1peak}, is determined using the FFT technique. Next, the peak value of the fundamental capacitive current is written as,

$$I_{c1peak} = I_{t1peak} \cos(\phi_{c1t1}) \tag{3.1}$$

where ϕ_{c1t1} is the phase shift between the fundamental components of the total arrester current and the capacitive current.

Since the fundamental component of the total arrester current contains a resistive component, the capacitive component leads i_{t1} and therefore, ϕ_{c1t1} is always positive. As an initial approximation, a small phase shift, δ is selected for ϕ_{c1t1}. The corresponding peak value of I_{c1} is calculated from Equation (3.1). The capacitive current so obtained is subtracted from the total arrester current to find the *generated resistive current.* The phase shift between the peak values of the *generated resistive* and capacitive currents is compared with the phase shift criterion. If the criterion is not satisfied, the value of ϕ_{c1t1} is increased in small steps and the procedure is repeated until the correct phase shift is obtained. The flowchart for the procedure is shown in Figure 3.9. The *generated resistive current*, thus obtained, may be used for diagnostic purposes.

3.5.2 Application of alternative diagnostic technique

The above technique was applied on the recorded waveforms of arrester currents obtained with actual arresters and valve elements (Sets A, B and C). For Set-A, the average phase shift was 76.6^o and two average values were considered for Set-B based on the phase shift versus voltage characteristics shown in Fig.3.7; 73.3^o at 0.8 pu of MCOV and 77.5^o at 0.9

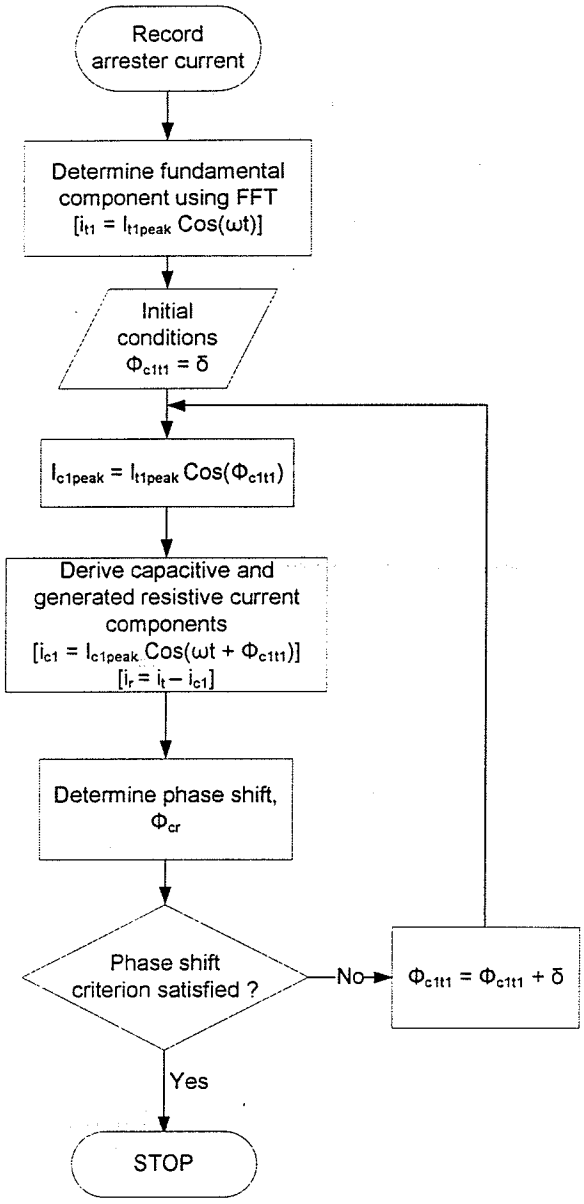

Figure 3.9: Flowchart of the iterative procedure suggested in Section 3.5.1

and 1.0 pu of MCOV. For Set-C, results were obtained for the two cases, mentioned in Table 3.3. by taking an average phase shift of 77.8°. The results are compared with the results obtained using the Compensation Technique in Table 3.4. The *generated resistive current*

waveforms obtained for the unaged sample of Set-A at its MCOV are shown in Figure 3.10.

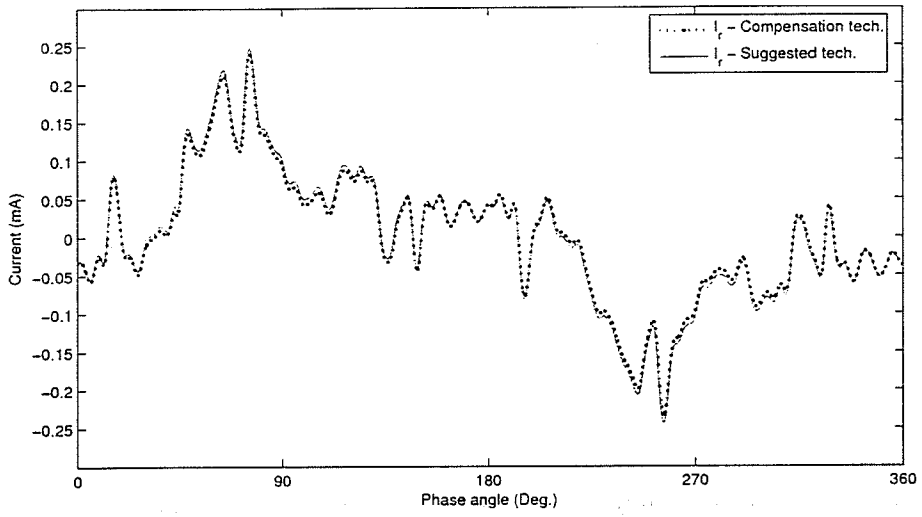

Figure 3.10: Comparison of generated resistive current wave shapes obtained using the suggested technique and the Compensation Technique (Unaged sample of Set - A at its MCOV)

3.5.3 Discussion of results

Table 3.4 shows that the application of the proposed diagnostic technique to Set-A yields *generated resistive current* magnitudes, which compare well with those obtained by use of the Compensation Technique. Aging can be therefore clearly identified by consideration of the peak value of the *generated resistive current.* Difficulties may occur due to change in phase shift criterion with Set-B (Fig.3.7). Although the phase shift criterion does not change due to voltage harmonics, the peak value of the *generated resistive current* may change as evidenced by examination of the results shown in Table 3.4 corresponding to cases 1 and 2 (see Table 3.2). For Set-C, the peak value of the *generated resistive current* obtained for Case 1 and 2 at its MCOV are 202 and 145 μA respectively. The change in the peak value of the *generated resistive current* due to the effect of harmonics is more than 25%. The effect of capacitive harmonics on the peak value of the *generated resistive current* is illustrated in Figure 3.11. Two harmonic conditions mentioned in Table 3.2 are considered.

Table 3.4: Comparison of results - generated resistive current

Voltage pu of MCOV	Set		$I_{rpeak}(\mu A)$ Comp. Tech.	$I_{rpeak}(\mu A)$ Suggested Tech.
0.8	Set-A	Unaged	142	139
		Aged-1	160	164
		Aged-2	225	232
	Set-B	Arrester1	92	97
		Arrester2	85	95
	Set-C	Case1	124	128
		Case2	85	98
0.9	Set-A	Unaged	178	173
		Aged-1	233	239
		Aged-2	318	319
	Set-B	Arrester1	147	148
		Arrester2	120	124
	Set-C	Case1	143	141
		Case2	108	113
1.0	Set-A	Unaged	240	243
		Aged-1	338	344
		Aged-2	513	515
	Set-B	Arrester1	218	253
		Arrester2	192	216
	Set-C	Case1	208	202
		Case2	145	148

The pure *resistive current* was derived using the Modified Compensation Technique for each case. Even though the peak value of pure *resistive current* is the same for the two cases, the *generated resistive current* using the proposed technique gives quite different peak values. Therefore, the peak value of the generated waveform, as a diagnostic indicator, is ineffective. In this case, the peak value of the *fundamental resistive current* can be used as a reference to distinguish the aging and harmonic effects, since the *fundamental resistive current* is insensitive to the voltage harmonics. The use of the fundamental component of the resistive current as a diagnostic indicator is discussed in detail in Chapter 4.

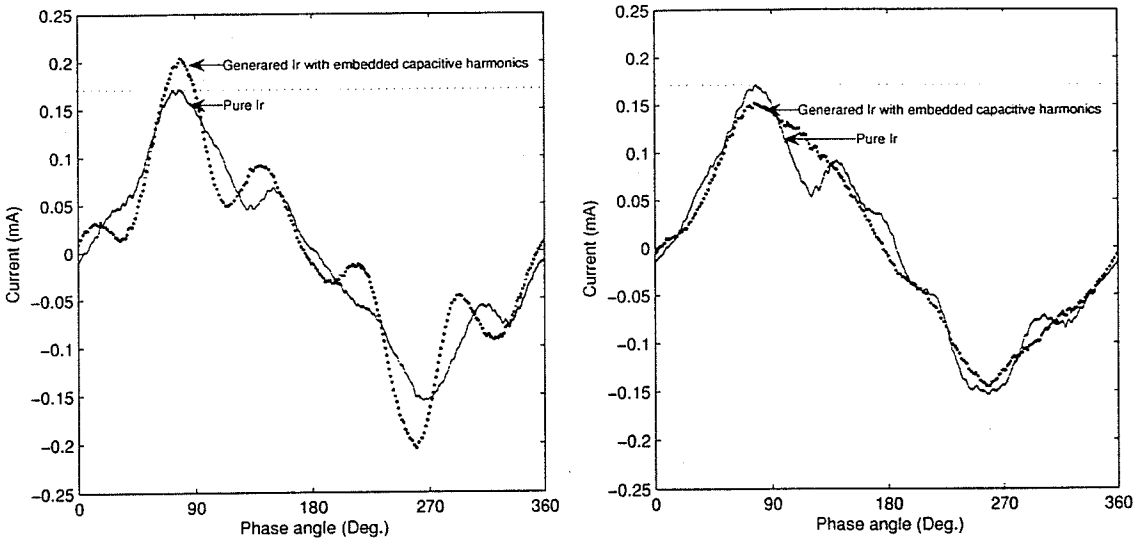

(a) Case 1 (b) Case 2

Figure 3.11: Comparison of resistive currents of Set-C at MCOV under two different harmonic conditions

3.5.4 Sensitivity of generated resistive current to measured phase shift

Since the magnitude of the *generated resistive current* is very small compared to that of the capacitive current, the error in the peak value of the *generated resistive current* may be considerable for a small change in the phase shift. The sensitivity of the diagnostic indicator to the phase shift can be evaluated as follows.

The change in the peak value of the *generated resistive current* for a small change in the phase difference between the peak of the capacitive current and the peak of the *generated resistive current* is given by,

$$\Delta I_{gr,peak} \approx \frac{\partial I_{gr,peak}}{\partial \phi_{cr}} \Delta \phi_{cr} \tag{3.2}$$

Where ϕ_{cr} is the phase difference between peaks of the capacitive and generated resistive current components.

By substituting $I_{gr,peak} = i_t(@I_{gr,peak}) - I_{c1,peak}\cos(\phi_{cr})$ in (3.2),

$$\Delta I_{gr,peak} \approx I_{c1,peak} \sin(\phi_{cr}) \Delta\phi_{cr} \tag{3.3}$$

Consider the following results obtained for Set-A (Unaged sample); $I_{gr,peak} = 240\mu A$, $I_{c1,peak} = 1.1mA$ and the average value of $\phi_{cr} = 76.6^o$. From (3.3),the percentage error in $I_{r,peak}$ for one degree change in ϕ_{cr} is 7.8%.

3.5.5 Implementation aspects

The peak position of the *generated resistive current* has to be determined precisely in order to obtain a good accuracy. It is impractical to measure the total arrester current on-line by employing a dropping resistor. A suitably designed current monitor may be preferable. Accuracy can be further improved by obtaining an average over a few successive cycles. Pre-determination of the phase shift characteristics at laboratory is required. The correct phase shift should be selected based on the system voltage.

Chapter 4

On-Line Assessment of Degradation of MOSA - A New Approach

In this chapter, a new method to assess the condition of Metal-Oxide Surge Arresters (MOSA) is presented, which uses the *fundamental resistive current* as a diagnostic indicator. In the proposed method, the arrester current is measured and its fundamental component derived using the Fast Fourier Transform (FFT). The *fundamental resistive current* is obtained by exploiting the linear relationship, which was found to exist between the peak value of the *fundamental resistive current* and the phase shift between the fundamental components of the capacitive current and the total arrester current. This relationship is shown in this work to be independent of temperature and arrester condition for a given type of arrester. Since only the fundamental components are considered, voltage harmonics do not affect the results. Also, since only the *fundamental resistive current* increases as a result of aging due to moisture ingress and oxygen reduction [15], it is a suitable indicator to detect this type of aging in addition to that caused by the cumulative effect of discharging impulse currents and internal partial discharges.

Results are presented to demonstrate the accuracy and the reliability of the new technique.

4.1 Basis of New Technique

4.1.1 I_{r1peak} - ϕ_{c1t1} characteristics of MOSA

The proposed new technique utilizes a unique relationship that exists between the peak value of the *fundamental resistive current* and the phase shift between the fundamental component of the capacitive current and the fundamental component of the total arrester current.

The experimental results obtained for the three sets of test objects (Set-A,B and C) mentioned in Chapter 3, were used to derive the I_{r1peak} - ϕ_{c1t1} characteristics. First, the Modified Compensation Technique was applied to derive the fundamental capacitive current from the measured total arrester current and the fundamental component of the applied voltage, which is derived form the measured voltage waveform, using the FFT technique (see Appendix B). Next, the *generated resistive current* was obtained and finally, the *fundamental resistive current* was derived from the *generated resistive current*, using the FFT technique. The fundamental current waveforms of the unaged sample of Set-A are shown in Figure 4.1. The phase shift between fundamental components of the capacitive current and the total arrester current, ϕ_{c1t1}, is also shown.

In the following, the dependence of these characteristics on MOSA condition, temperature, arrester type and voltage harmonics is discussed.

4.1.2 Dependence of I_{r1peak} - ϕ_{c1t1} characteristics on arrester condition

The valve elements of Set-A were tested under different applied voltages in the range of 0.8 to 1.2p.u. of MCOV. The I_{r1peak} - ϕ_{c1t1} characteristics were obtained by applying the technique explained in Section 4.1.1. From the results shown in Figure 4.2, it is found that the characteristics are the same for all three samples and therefore the relationship is

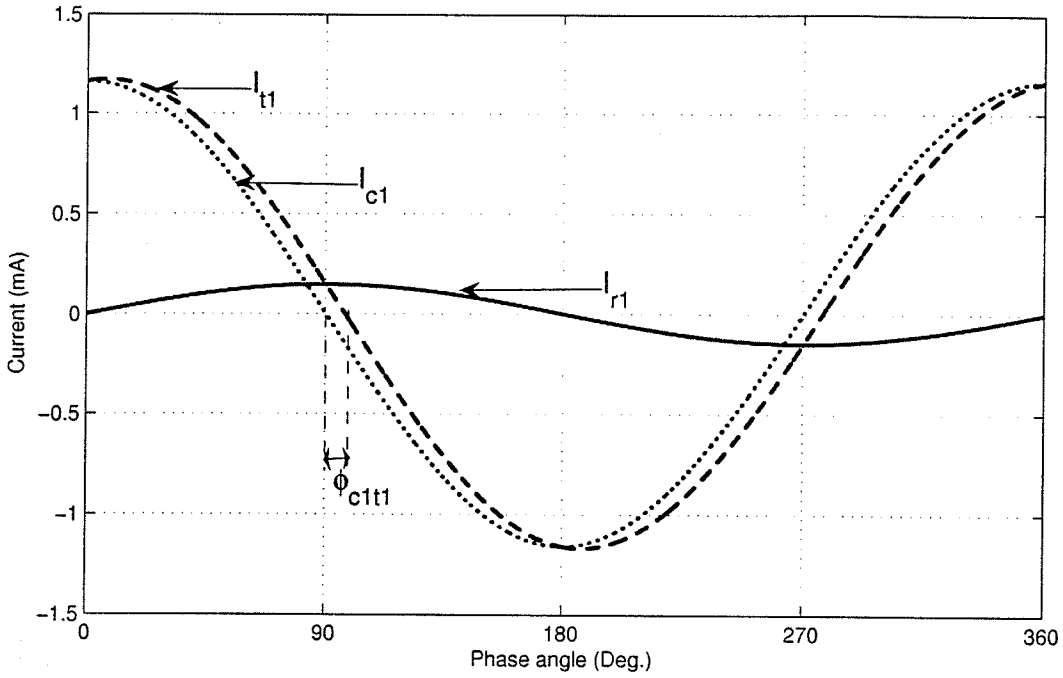

Figure 4.1: Fundamental components of total, capacitive and resistive currents of an unaged set of valve elements at its MCOV

independent of MOSA condition.

4.1.3 Dependence of I_{r1peak} - ϕ_{c1t1} characteristics on temperature

The steady state operating temperature of surge arresters may change due to change in ambient temperature and/or aging. Short duration temperature rise may also occur due to lightning impulses and temporary over voltages. The arresters are usually tested on-line for aging in the summer period and therefore the operating temperature may be considered greater than 20^oC. In order to analyze the effect of arrester temperature on the derived characteristics, the valve elements in Set-A were tested at four different temperatures, 23^oC, 50^oC, 70^oC and 100^oC. The test results (Figure 4.3) show that the change in the characteristics due to temperature change is negligible in the temperature range of 23 *to* 100^oC.

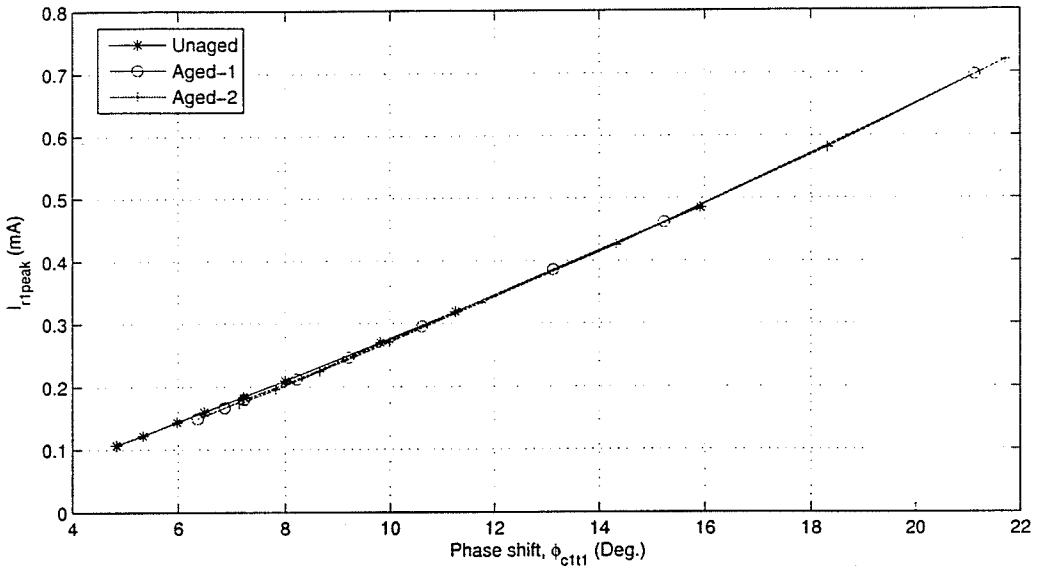

Figure 4.2: I_{r1peak} versus ϕ_{c1t1} characteristics in the range of 0.8 to 1.2p.u. of MCOV for Set-A at 23^oC.

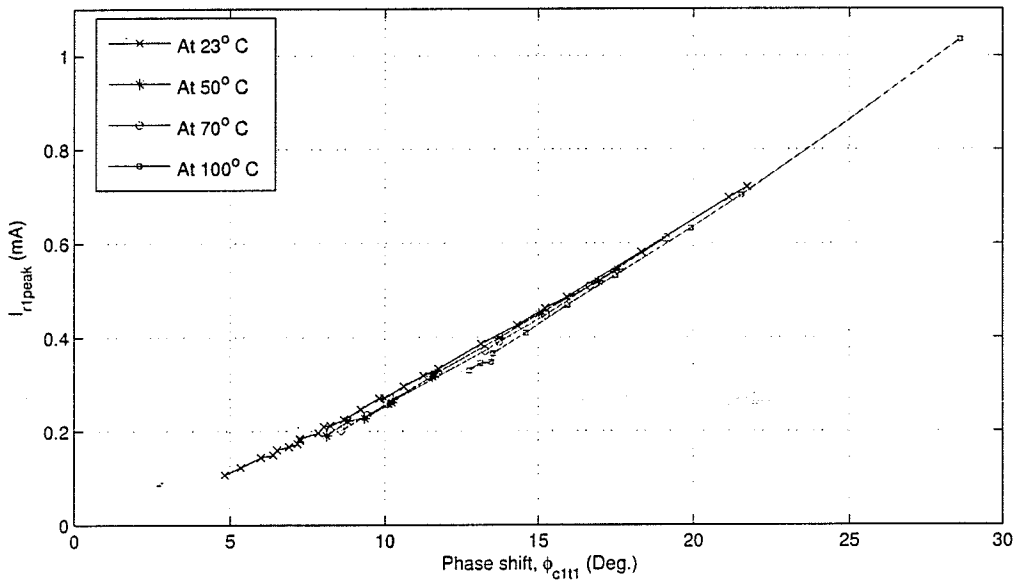

Figure 4.3: I_{r1peak} versus ϕ_{c1t1} characteristics at 23^oC, 50^oC, 70^oC and 100^oC in the range of 0.8 to 1.2 p.u. of MCOV.

4.1.4 Dependence of I_{r1peak} - ϕ_{c1t1} characteristics on arrester type

The characteristics were also derived for complete arrester units of Set-B. Results obtained by using two similar arresters are compared in Figure 4.4. This verifies that the character-

istics are unique for a particular arrester type.

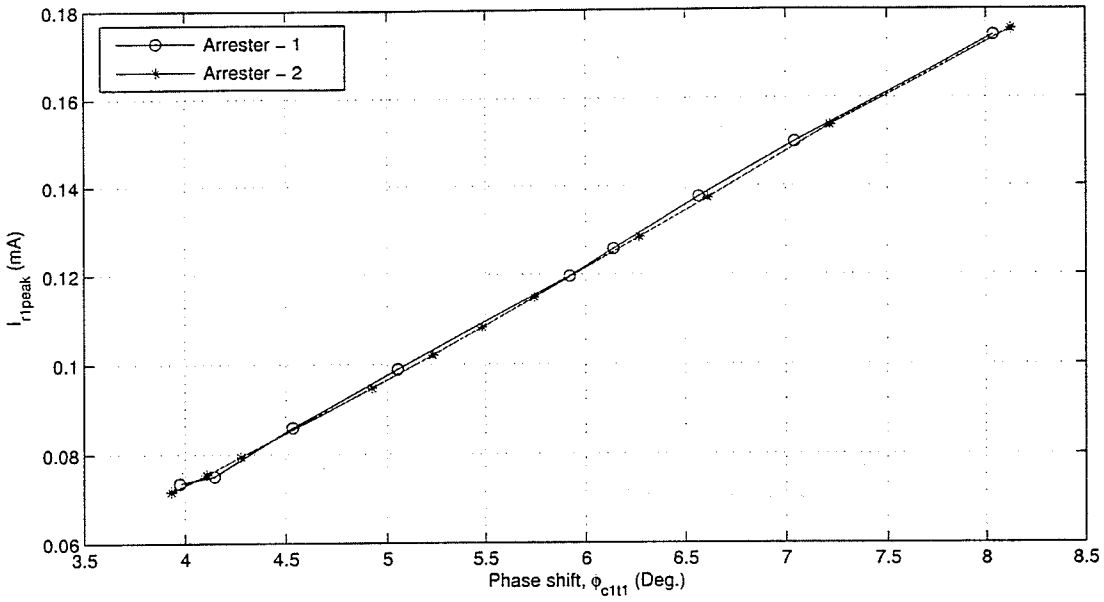

Figure 4.4: I_{r1peak} versus ϕ_{c1t1} characteristics for Set-B in the range of 0.8 to 1.1 p.u. of MCOV

4.1.5 Dependence of I_{r1peak} - ϕ_{c1t1} characteristics on voltage harmonics

The total harmonic distortion of system voltage is usually within ±5% and the harmonic introduced current in the *fundamental resistive current* is negligible. Since this relationship involves fundamental components, voltage harmonics do not affect the characteristics.

4.1.6 Application of I_{r1peak} - ϕ_{c1t1} characteristics in diagnosis

The above analysis shows that the I_{r1peak} - ϕ_{c1t1} characteristic is unique for a particular arrester type and it is independent of arrester condition, harmonics and temperature. For example, suppose that the nominal system voltage applied to an arrester is 0.85 of MCOV. The steady state system voltage may vary by ±5% , i.e., in the range of 0.8 to 0.9 of MCOV. The I_{r1peak} - ϕ_{c1t1} characteristics in the above voltage range are shown in Figure 4.5 for the aged and unaged samples of Set-A. A linear approximation fits the characteristics obtained

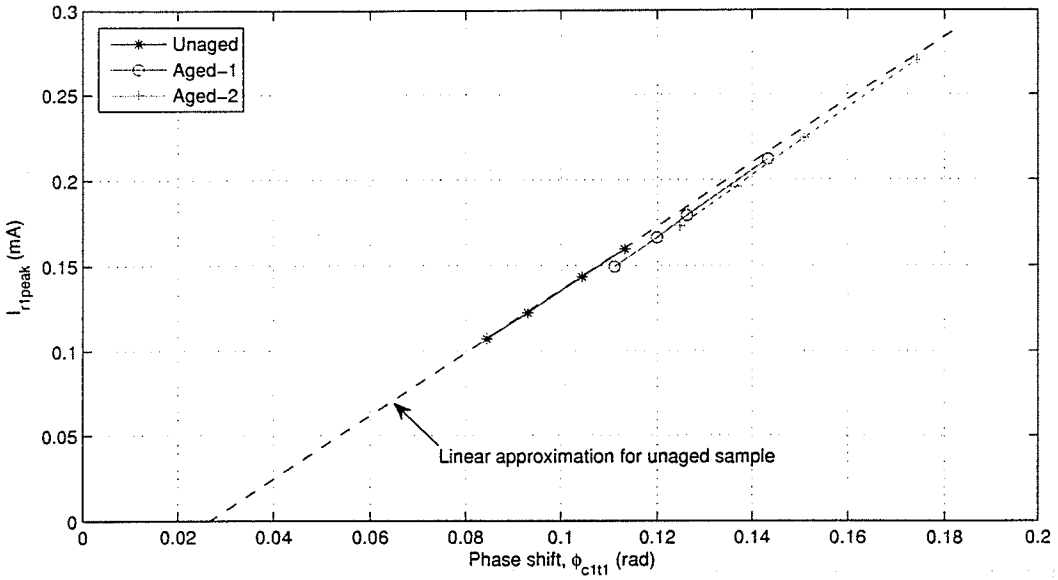

Figure 4.5: I_{r1peak} versus ϕ_{c1t1} characteristics for Set-A in the range of 0.8 to 0.9 p.u. of MCOV - linear approximation

with the unaged sample. A little deviation can be observed for the characteristics obtained with the aged samples. The maximum deviation from the linear approximation is about $8\mu A$. A general form of linear approximation can be given as in Equation (4.1), where ϕ_{c1t1} is in radians and I_{r1peak} is in mA and A, B are constants to be determined by testing the arrester in a laboratory at a few different voltages. For the linear approximation shown in Figure 4.5, $A = 1.8458mA(peak)/radians$ and $B = -0.0492mA(peak)$.

$$I_{r1peak} = A * \phi_{c1t1} + B \tag{4.1}$$

4.2 Suggested new diagnostic procedure

1. The total arrester current is recorded and its fundamental component is determined using the FFT technique without knowledge of the applied voltage.

2. The *fundamental resistive current* is determined iteratively as follows.

- The peak value of the *fundamental resistive current*, I_{r1peak}, is related to the peak value of the fundamental component of the total arrester current, I_{t1peak}, as indicated by (4.2).

$$I_{r1peak} = I_{t1peak} \sin(\phi_{c1t1}) \tag{4.2}$$

  For a particular arrester current measurement, Equation (4.2) yields the I_{r1peak} versus ϕ_{c1t1} characteristics, which is identified by curve "A" in Figure 4.6. It should be noted that the sinusoidally varying curve "A" is not a current waveform. Rather, it represents a characteristic relation and only one point on this curve is of interest. This point represents the operating point, which is found by simultaneous solution of Equation (4.2) (curve A) and Equation (4.1) (line B). The peak value of the *fundamental resistive current* is therefore, in Figure 4.6, at the intersection of curve A and line B.

- The Method of Successive Substitution is used to arrive at the operating point from an initial approximation of the value of ϕ_{c1t1} when $I_{r1peak} = 0$ (i.e. $\phi_{c1t1} = -B/A$ from Equation (4.1)). For this value of ϕ_{c1t1}, a new I_{r1peak} is found from Equation (4.2). The resultant I_{r1peak} is substituted in Equation (4.1) to find the next value of ϕ_{c1t1}.The iterative procedure is repeated; the solution for ϕ_{c1t1} converges to the operating point. It is found that the number of iterations required is less than 50. The successive iterations are interpreted graphically by dotted line in Figure 4.6. The flowchart of the new technique is shown in Figure 4.7.

- The same procedure is repeated for a few successive cycles of measured arrester current and the mean waveform of the derived *fundamental resistive currents* determined for better accuracy.

3. The *fundamental resistive current* so determined can be used as a diagnostic indicator. Section 4.3 discuses use of the *fundamental resistive current* as a diagnostic indicator.

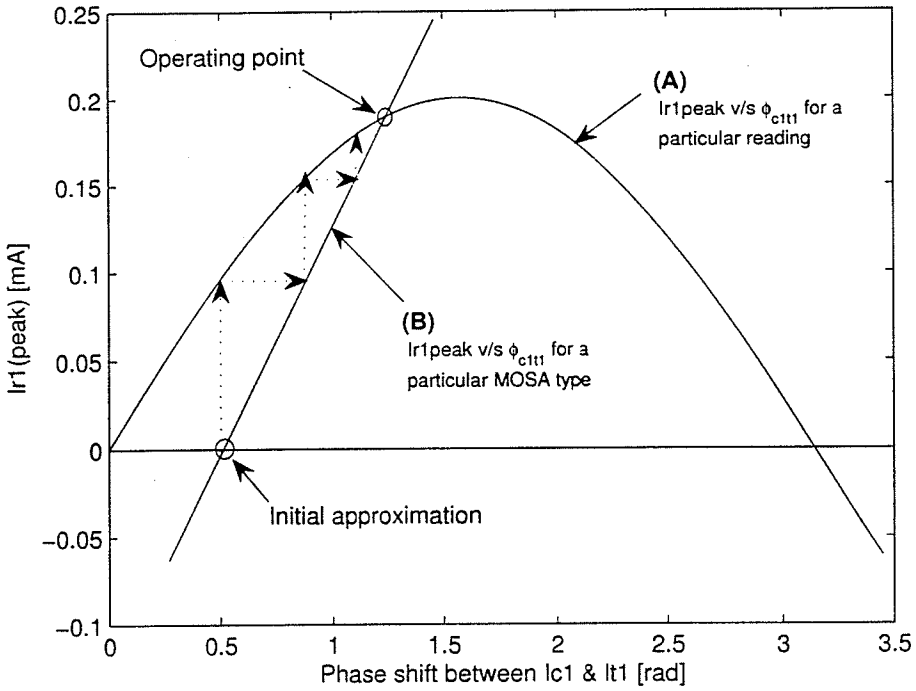

Figure 4.6: Method of solving equations 4.2 and 4.1. (Schematic diagram; axes are not to scale)

4.3 Fundamental resistive current as a diagnostic indicator

As mentioned in introductory section, the *resistive component* of the arrester current reflects the condition of MOSA. In literature, either the peak value of the *generated resistive current* or the 3^{rd} harmonic component of the *resistive current* has been used in on-line diagnosis. The conventional equivalent circuit in which a MOSA is represented by a non-linear resistor in parallel with a capacitor, is used to derive these currents. Although it is expected that the resistive current should be in-phase with the applied voltage, there is a considerable phase shift (about 10 *to* 20^o) in the low electric field region as mentioned in Chapter 3. Therefore, the use of conventional equivalent circuit to derive the *resistive current* in low electric field region is suspect [11].

In this method, the peak value of the *fundamental resistive current* is derived accurately

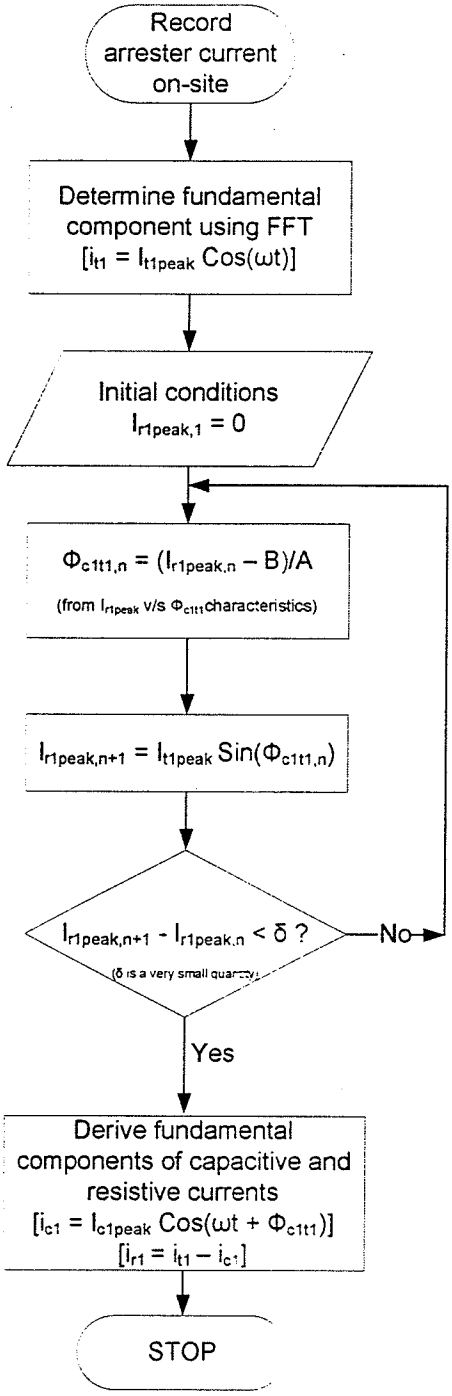

Figure 4.7: Flowchart of the new on-line applicable technique

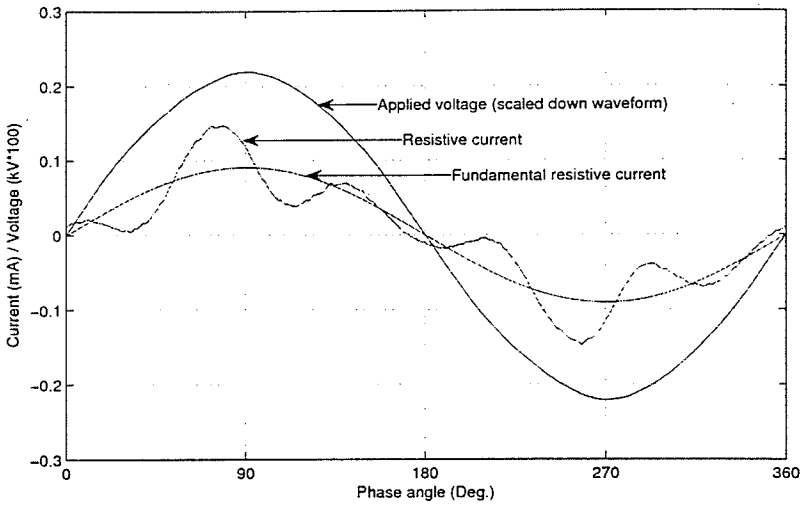

Figure 4.8: Applied voltage, resistive current and fundamental resistive current waveform of a MOSA at its MCOV

and used as an indicator. It is found (Figure 4.8) that the derived *fundamental resistive component* is in-phase with the applied voltage. Although the conventional equivalent circuit yields a *resistive current*, which is not in-phase with the applied voltage, it generates the *fundamental resistive component* accurately.

In order to check the feasibility of use of *fundamental resistive current* as a diagnostic indicator, it was compared with the associated power loss in the arrester. Table 4.1 shows the increase in the *fundamental resistive current* for aged and very aged valve elements of Set-A as a percentage of the corresponding values obtained with unaged valve elements at 3 selected values of applied voltage. Table 4.2 shows similar results for the associated power loss. The average power loss was calculated numerically using Equation 4.3. A comparison shows that the peak value of the *fundamental resistive current* is well correlated with the power loss, which in turn reflects the condition of valve element.

$$P_{loss} = \frac{1}{T}\int_0^T v i_r dt \tag{4.3}$$

Table 4.1: Peak value of fundamental resistive current of aged samples expressed as percentage of corresponding peak value of fundamental resistive current of unaged sample

Voltage	Ir1 peak (%) Unaged	Ir1 peak (%) Aged-1	Ir1 peak (%) Aged-2
0.8 MCOV	100	139.7	162.0
0.9 MCOV	100	132.6	156.3
MCOV	100	133.7	180.8

Table 4.2: Power loss of aged samples expressed as percentage of corresponding loss of unaged sample

Voltage	Power loss (%) Unaged	Power loss (%) Aged-1	Power loss (%) Aged-2
0.8 MCOV	100	139.8	161.7
0.9 MCOV	100	133.1	155.3
MCOV	100	133.6	181.0

4.4 Results and Discussion

For SET-A, the I_{r1peak} - ϕ_{c1t1} characteristics were derived by using the test results of the unaged sample. The same characteristics were used to implement the new technique for the aged sample as well. Both samples were tested under voltages in the range 0.8 to 1.0 pu of MCOV. Results derived using the new technique are presented in Figure 4.9. There is a clear margin between the results of the unaged sample and those of aged samples. The aging can be clearly identified.

The new technique was also applied to the test results of complete arrester units of SET-B. The I_{r1peak} - ϕ_{c1t1} characteristics were obtained by using test results of one of the arresters. Results of the new technique, which are illustrated in Figure 4.10 are almost the same for the both of the arresters. This confirms that the characteristics defined are unique for a particular arrester type.

SET-C was tested under different harmonic conditions of the applied voltage mentioned in Table 3.2. Figure 4.11 shows the *generated resistive current* and the *fundamental resistive current* components obtained for SET-C under two different harmonic conditions. Although

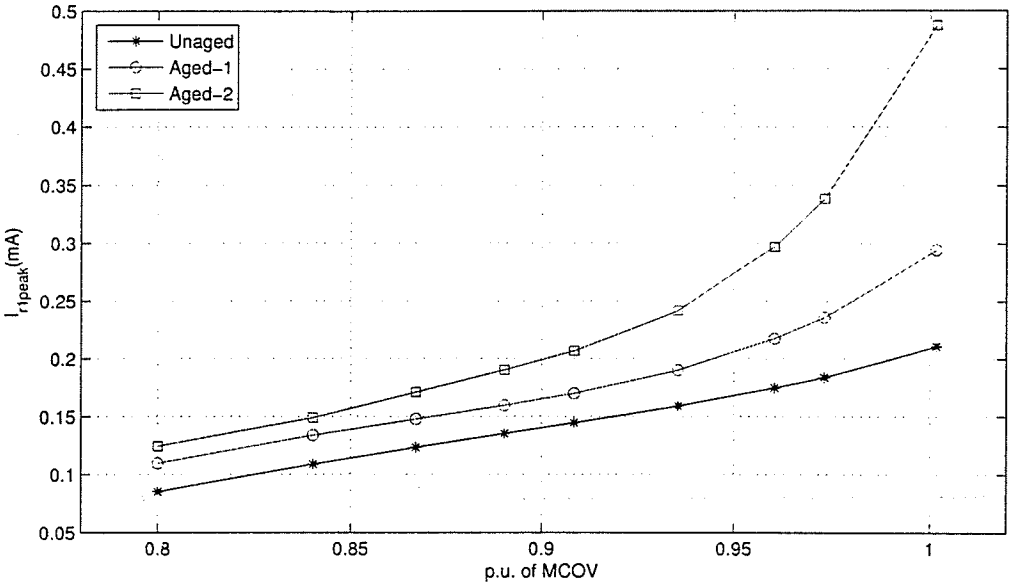

Figure 4.9: Variation of I_{r1peak} with voltage for SET-A

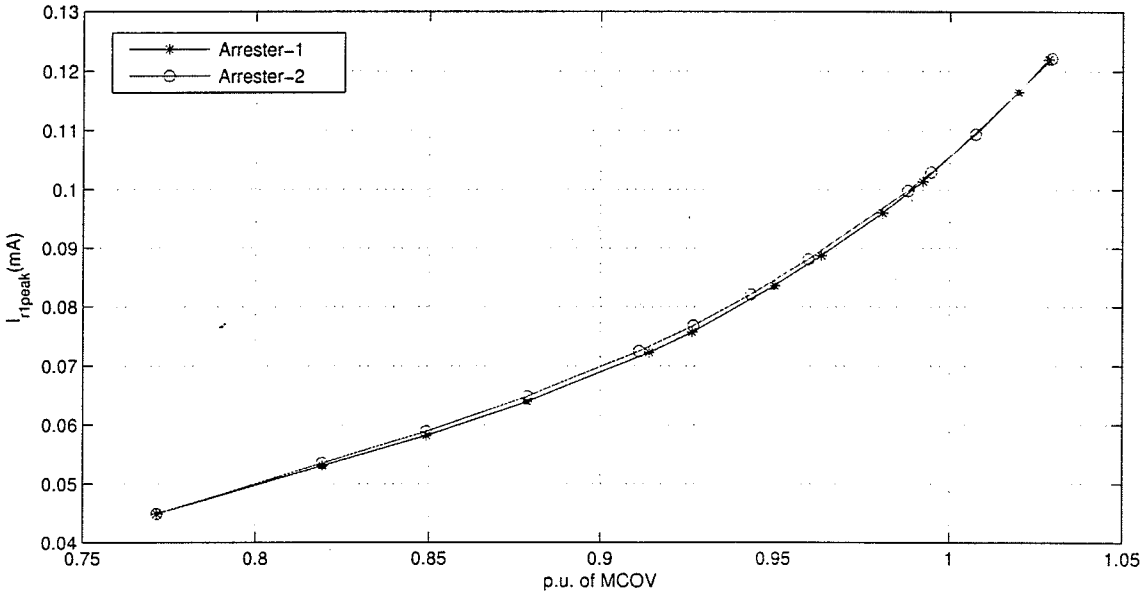

Figure 4.10: Variation of I_{r1peak} with voltage for SET-B

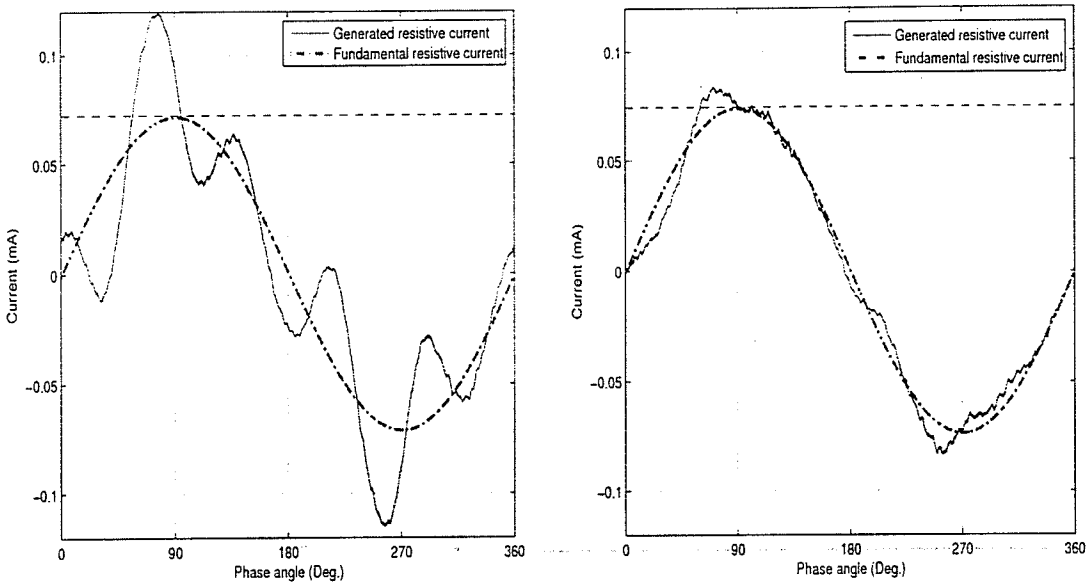

(a) Case 1 (b) Case 2

Figure 4.11: Resistive current and fundamental resistive current for SET-C under different harmonic conditions.

there is considerable difference in the peak values of the *generated resistive currents* the fundamental components derived by the new technique are almost the same and there is no effect of voltage harmonics on the new technique.

Finally, in Table 4.3, the results obtained for all three sets at their MCOV are compared with the results obtained by use of the Compensation Technique. Results obtained by application of the new technique agree well with those obtained by use of the compensation technique. Since only the fundamental component of the total current is used, measuring errors due to noise are negligible and therefore, the reliability is also high.

4.5 Sensitivity Analysis For Suggested Method

The change in the peak value of the *fundamental resistive current* for a small change in phase shift between the fundamental component of the capacitive current and the fundamental component of the total current is given by.

Table 4.3: Comparison of results - fundamental resistive current

Voltage pu of MCOV	Set		$I_{r1peak}(\mu A)$ Comp. Tech.	$I_{r1peak}(\mu A)$ New Tech.
0.8	Set-A	Unaged	110	110
		Aged-1	149	140
		Aged-2	173	160
	Set-B	Arrester1	56	55
		Arrester2	55	53
	Set-C	Case1	74	71
		Case2	72	74
0.9	Set-A	Unaged	148	144
		Aged-1	179	177
		Aged-2	224	222
	Set-B	Arrester1	75	72
		Arrester2	74	74
	Set-C	Case1	86	85
		Case2	89	86
1.0	Set-A	Unaged	184	184
		Aged-1	246	234
		Aged-2	333	333
	Set-B	Arrester1	100	101
		Arrester2	108	101
	Set-C	Case1	110	108
		Case2	109	106

$$\Delta I_{r1,peak} \approx \frac{\partial I_{r1,peak}}{\partial \phi_{c1t1}} \Delta \phi_{c1t1} \tag{4.4}$$

By substituting (4.2) in (4.4),

$$\Delta I_{r1,peak} \approx I_{c1,peak} \Delta \phi_{c1t1} \tag{4.5}$$

In this method, deviation of ϕ_{c1t1} from its actual value is very small. It is found experimentally that the root mean square deviation of ϕ_{c1t1} is less than 0.4 Deg.

Consider the following results obtained for Set-A (Unaged sample); $I_{r1,peak} = 184\mu A$, $I_{c1,peak} = 1.1mA$. Therefore, from (4.5), the mean percentage error. which may occur in $I_{r1,peak}$ is less than 5%.

4.6 Implementation Aspects

4.6.1 Suggested design

The basic block diagram of the suggested design is illustrated in Figure 4.12. This design can be used with the new technique as well as the method suggested in Chapter 3. The functional details of each block are given below.

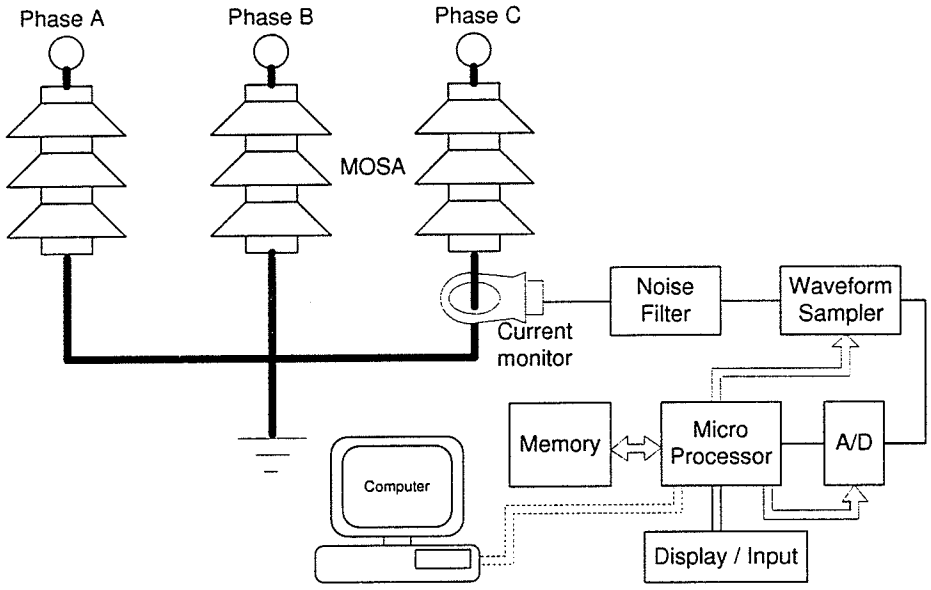

Figure 4.12: Suggested design - basic block diagram

Current Monitor: This includes a properly designed clip-on type current transformer, which is able to measure μA range arrester currents and a current to voltage amplifier, which converts the measured current signal into a voltage signal.

Noise filter: This is a low pass filter, which removes high frequency noise embedded in the measured signal.

Waveform sampler: Once the instructions from the micro processor received, the Waveform sampler samples one cycle of the measured signal and passes it to the A/D converter.

A/D converter: The sampled analog waveform is converted into a digital signal.

Micro processor: This is the main processing unit of the design. When the diagnosis starts in the field, a few successive cycles of the arrester current is stored in the memory by giving instructions to the waveform sampler and the A/D converter. Next, the processor runs the algorithm shown in Figure 4.7. The *fundamental resistive current*, which is the average of the results obtained from recorded waveforms, is displayed and compared with pre-defined values. All the derived waveforms are also stored in the memory. In off-line, the stored waveforms may be transferred in to a PC data base.

Display/Input: A touch panel display can be used. The measured and the derived waveforms may be displayed. The parameters of I_{r1peak} - ϕ_{c1t1} characteristics, temperature and rms system voltage are inserted manually.

Computer: The processor communicates with a PC off-line. In the computer, a data base is maintained for each arrester in the system. Further analysis of the transferred data and comparison with the historical data are possible.

4.6.2 Correction factors

The peak value of the *fundamental resistive current* will change with the arrester temperature and voltage. To identify the aging clearly, correction of the reference value (expected value for an unaged arrester) for voltage and temperature is required. While the diagnosis is performed, the system rms voltage can be read from the nearest substation. The arrester temperature may be roughly determined using an infra red thermal camera. The ambient temperature should also be recorded. The expected peak value of the *fundamental resistive current* for an unaged arrester may be predicted by using a proper correction algorithm, which takes voltage and temperature into account.

Chapter 5

Conclusions and Recommendations

Conclusions

The thesis has examined the arrester current based diagnostic techniques, which have on-line applicability. The *resistive current component*, which indicates the condition of an arrester, can be obtained based on the arrester current wave-shape characteristics without resorting to voltage waveform measurement; two techniques have been proposed.

The technique discussed in Chapter 3, is based on the constancy of the phase shift between the fundamental capacitive current and the *generated resistive current.* It is verified that the phase shift is sensibly constant and is independent of arrester condition and operating temperature. However tests on an actual station type arrester revealed that the phase shift is slightly higher at applied voltages greater than 0.85 of MCOV. In view of the sensitivity of the diagnostic indicator to phase shift it is important to use the correct phase shift value.

An iterative procedure [19], which is not the same as the one outlined in [15], has been clearly explained to arrive at the magnitude of the *generated resistive current*, which compares well with that obtained by use of the Compensation Technique (Bench Mark Method). The presence of voltage harmonics does not affect the phase shift, but may result in a different value of resistive peak current. In this case the peak value of the *fundamental*

resistive current may be used as a diagnostic indicator.

A new technique [18] in which the *fundamental resistive current* is used as a diagnostic indicator, has been proposed in Chapter 4. The elements of this technique are totally different from the procedure outlined in [15] or the modified procedure referred to above. In order to determine the *fundamental resistive current*, a unique relationship between the peak value of the *fundamental resistive current* and the phase shift between the fundamental component of the total current and the fundamental component of the capacitive current is derived (I_{r1peak} - ϕ_{c1t1} characteristic). This characteristic, which is central to the suggested diagnostic procedure, is independent of the condition of MOSA as well as its temperature up to 100^oC. Although it is possible that the temperature of the valve elements of an arrester can exceed 100^oC immediately after energy absorbtion, the suggested diagnostic procedure is applicable under normal conditions. An iterative technique is used to obtain the results, which compare well with the results obtained by use of the compensation technique (Benchmark method). Since this method involves only the fundamental components, the results are insensitive to voltage harmonics. Although, the conventional equivalent circuit, the accuracy of which is suspect in the low electric field region, is used in this technique, the derived *fundamental resistive current* is in-phase with the voltage, representing a pure resistive component. Therefore, the accuracy of the equivalent circuit is not of concern. If the arrester current is measured with a suitably designed current monitor the suggested method has on-line applicability.

Suggestions for Further Research

Further work is recommended as an extension of this thesis in the following areas:

1. The accuracy of the technique suggested in Chapter 3 depends on the precise positioning of the peak of the generated resistive current. The noise added to the arrester current in the field measurements may change the peak position of the generated resistive current, which leads to inaccurate results. Further analysis of the effect of noise

on the diagnostic technique is recommended.

2. The proposed diagnostic techniques were only tested with laboratory test setups. The techniques have to be verified with field tests.

3. The hardware implementation can be carried out as discussed in Chapter 4. A leakage current probe with a high sensitivity is required. In the software part, the correction factors may be added as discussed in Chapter 4. A sophisticated diagnostic instrument may be finally devised.

Appendix A

Laboratory Test Setup-Details

The valve elements and the arresters were tested at the laboratory using a test setup as mentioned in Chapter 2 and 3. A photograph of the setup is shown in Figure A.1.

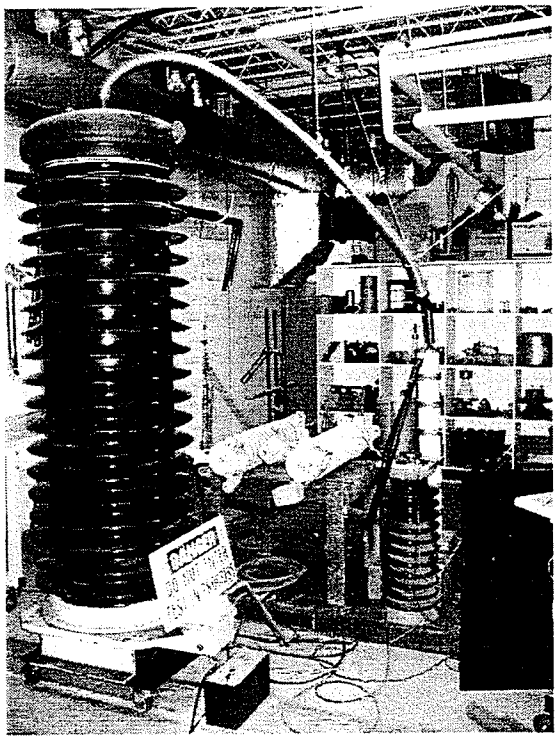

Figure A.1: Photograph of laboratory test setup

A.1 Voltage and current measurement

The applied voltage and the arrester current were measured using a capacitive divider/HV probe and a dropping resistor respectively (Figure A.2).Details of the equipments are given below.

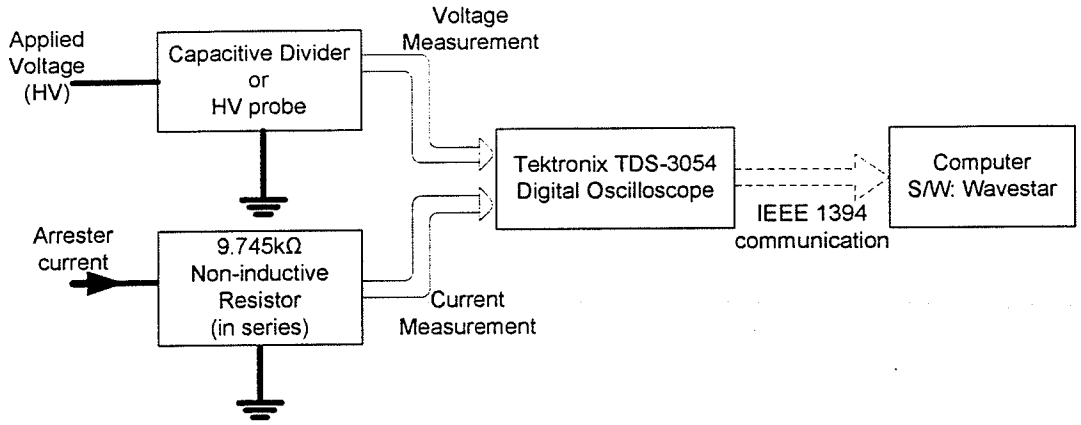

Figure A.2: Voltage and current measurement

1. Capacitive Divider:

   HV: Seven capacitors of $0.0025\mu F, 25kV$ in series; total of $357pF, 175kV$

   LV: Five capacitors of $0.082\mu F, 1000V$ in parallel; total of $0.41\mu F, 1000V$

   Ratio: 1150 : 1

2. Tektronix Passive High Voltage Probe P6015A:

   Band width: 75MHz

   Attenuation: 1000X

   Rise time: 4.0ns

   Loading: $100M\Omega/3pF$

   Rated voltage: 20kV rms

3. Tektronix TDS-3054 Digital Oscilloscope:

   Band width: 500MHz

Channels: 4

Sampling rate: 5GS/s

Vertical resolution: 9 bits

Input impedance: $1M\Omega$ in parallel with 13pF

4. WaveStar:

   The associated software with Tektronix oscilloscopes.

A.2 Data acquisition and process

The waveforms recorded by the oscilloscope were transferred to the PC and stored as a WaveStar file. A screen print of a recorded WaveStar file is shown in Figure A.3. Next, the recorded waveform data was converted into a CSV file using WaveStar. For the convenience, the CSV files were saved as Microsoft Excel work sheets.

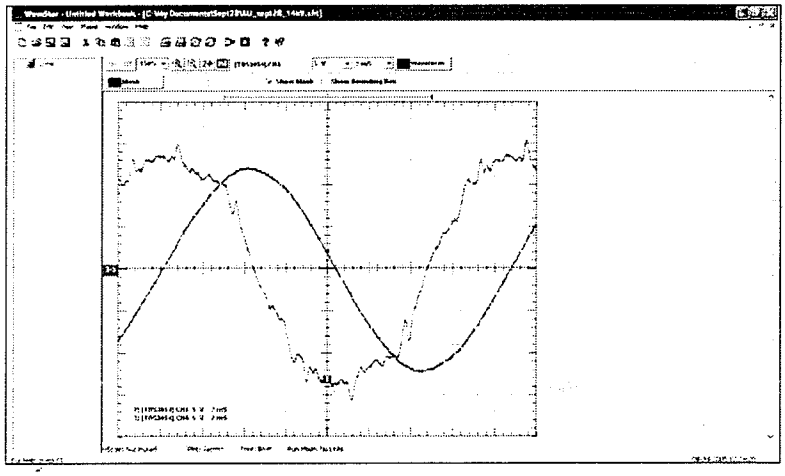

Figure A.3: Recorded voltage and current waveforms - WaveStar file

The Excel work sheets were read using a MATLAB code. The recorded waveforms contained high frequency noise components and they were removed using a Savitzky-Golay software filter, which is available in MATLAB image processing tool box. The filter performs an un-weighted linear least squares fit using a polynomial of a given degree for a given

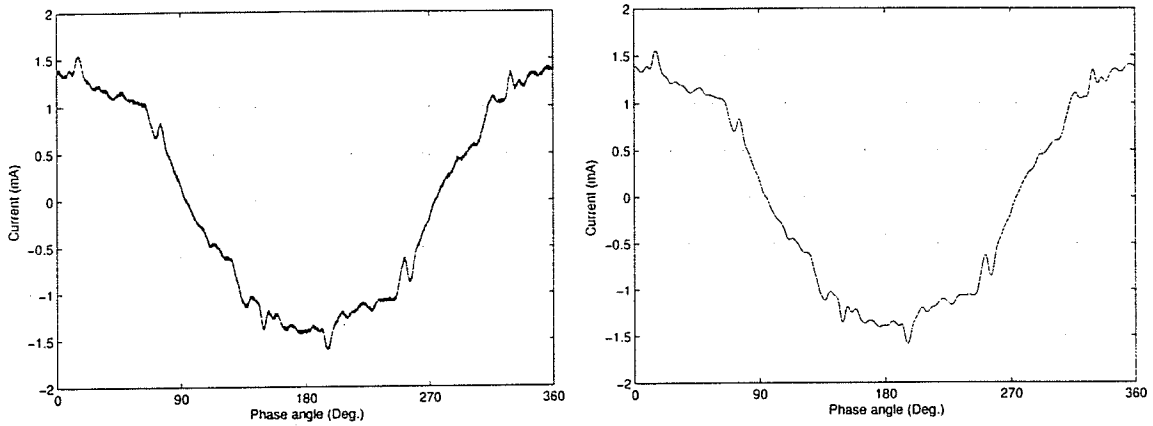

(a) Arrester current before filtering

(b) Arrester current after filtering

Figure A.4: Rejecting noise in arrester current - filter performance

spacing of data. The filter performance is illustrated in Figure A.4.

A.3 The Compensation Technique - MATLAB code

The MATLAB code of Compensation technique used to derive the capacitive and resistive components of the arrester current is given below.

```
%--------------------------     START     ---------------------------------
clear all
clc
%.................   Read Excel data file   ....................
data = xlsread('Input.xls');
dt = data(2,1)-data(1,1); % time step
T = 1/60;
vol_m = data(:,4); %Recorded voltage
curr_m = data(:,6);%Recorded current

%.....................  Noise Filtering  ......................
vol = sgolayfilt(vol_m,3,301);  %3rd-order filter, Spacing=301 data points
```

```
curr = sgolayfilt(curr_m,3,101);%3rd-order filter, Spacing=101 data points

%.............. Select one cycle of voltage ..................
i = 1;
while true
    if vol(i+1) > 0
        if vol(i) > 0
            start1 = i;
            break
        end
    end
    i = i+1;
end
i = start1 + fix(0.8*T/dt);
while true
    if vol(i+1) > 0
        if vol(i) > 0
            stop1 = i;
            break
        end
    end
    i = i+1;
end
vol_off = vol(start1:stop1);
steps = length(vol_off);

%.......... To find the average (DC) value of voltage ..........
intg = 0;
```

```
for i = 2:steps
    fa =  vol_off(i);
    fb =  vol_off(i-1);
    intg = intg + (fa + fb)/2;  %.... Trapizoidal rule
end
avg = intg/(stop1 - start1);
vol = vol - avg;   %..... Removing the dc component

%....... To find the average (DC) value of total current .........
curr_off = curr(start1:stop1);
intg = 0;
for i = 2:steps
    fa =  curr_off(i);
    fb =  curr_off(i-1);
    intg = intg + (fa + fb)/2;  %.... Trapezoidal rule
end
avg = intg/(stop1 - start1);
curr = curr - avg;   %..... Removing the dc component

%....... Select a one cycle of offset removed voltage ............
i = 1;
while true
    if vol(i+1) > 0
        if vol(i) > 0
            start = i;
            break
        end
    end
```

```
    i = i+1;
end
i = start + fix(0.8*T/dt);
while true
    if vol(i+1) > 0
        if vol(i) > 0
            stop = i;
            break
        end
    end
    i = i+1;
end

%........  FFT to find the fundamental of the voltage  ..........
vol_fft = vol(start:stop);
steps = length(vol_fft);
time = dt*(0:(steps - 1))';
fft_V = fft(vol_fft);
mag = abs(fft_V)*2/steps;
phase = unwrap(angle(fft_V));
freq = 1/(dt*steps);
vol_f = (mag(2)*cos(2*pi*freq*time'+phase(2)))'; % V_f

vol_c = (mag(2)*cos(2*pi*freq*time'+phase(2)+pi/2))';% phase shifted V_f
curr_c= curr(start:(start+steps-1));

%..................... Finding minimum G .......................
min = 10000;
```

```
for G = 0.4:0.0001:1.4
    int = 0;
    for i = 2:steps(1,1)
        fa = (curr_c(i) - G*vol_c(i))* vol_c(i);
        fb = (curr_c(i-1) - G*vol_c(i-1))* vol_c(i-1);
        int = int + (fa + fb)*dt/2;

    end
    if abs(int) < min
       min = int;
       Gmin = G;
    end
end
display(Gmin);

%.......................... Finding Ic.........................
val = zeros(1:steps,1);
a = 2;
for j = 1:10 % to consider Ic harmonics
   val = val+Gmin*(a-1)*(mag(a)*cos(2*pi*freq*(a-1)*time'+phase(a)+pi/2))';
   a=a+1;
end
It = curr_c;        % total arrester current
Ir = curr_c - val; %Resistive current
Ic = curr_c - Ir;  %capacitive current
phs = time'*(2*180/((steps-1)*dt));

%.............. Writing the results to a Excel file ...........
```

```
xlswrite('results.xls',[phs',vol(start:stop), vol_f, It, Ic, Ir]);


%.................. Display derived waveforms ..................
plot(phs,[vol(start:stop),It,Ir,Ic]');
hold on;
grid on;
%---------------------------  STOP  -----------------------------------
```

Appendix B

Fast Fourier Transform

B.1 Fourier Transform

The Fourier transform is used to transform a continuous time domain signal into the frequency domain. It describes the continuous frequency spectrum of a non-periodic time signal. The Fourier transform, $X(f)$ of a continuous time function $x(t)$ can be expressed as,

$$X(f) = \int_{-\infty}^{\infty} x(t)\ e^{-j2\pi ft} dt \tag{B.1}$$

And the inverse transform is given by,

$$x(t) = \int_{-\infty}^{\infty} X(f)\ e^{j2\pi ft} df \tag{B.2}$$

B.2 Discrete Fourier Transform

This is the method used to transform a discrete time domain signal (a sampled signal) into the frequency domain. In this case the frequency domain is also discrete. Let $x(nT)$ represent the discrete time signal, and let X(mF) represent the discrete frequency transform function. The Discrete Fourier Transform (DFT) is given by,

$$X(mF) = \sum_{n} x(nT)\ e^{-jnm2\pi FT} \tag{B.3}$$

And the inverse transform is given by,

$$x(nT) = \frac{1}{N} \sum_{m} X(mF)\ e^{jnm2\pi FT} \tag{B.4}$$

where N is the number of samples and T is the sampling rate. $F = \frac{1}{NT}$.

B.3 Fast Fourier Transform

The fast Fourier transform (FFT) is simply a class of special algorithms, which implement the discrete Fourier transform with considerable savings in computational time. It must be pointed out that the FFT is not a different transform from the DFT, but rather just a means of computing the DFT with a considerable reduction in the number of calculations required. For example, the technique used in MATLAB is based on an algorithm called "Cooley-Tukey".

References

[1] T.K. Gupta "Application of Zinc Oxide Varistors", *Journal of the American Ceramic Society*, Vol. 73, No. 7, 1990, pp. 1817-1840.

[2] L.M. Levinson (Editor): "Electronic Ceramics - Properties, Devices and Applications", Marcel Dekker Inc, New York, 1988

[3] A. Schei et K.H. Weck, "Metal Oxide Surge Arresters in AC Systems Part1: General properties of the metal oxide surge arrester", *Electra*,No. 128, 990, p100-105.

[4] Kazuo Eda, "Conduction Mechanism of Non-Ohmic Zinc Oxide Ceramics", *Journal of Applied Physics*,Vol. 49, No. 5, 1978, p2964-2972.

[5] M. Bartkowiak, M.G. Comber and G.D. Mahan, "Failure Modes and Energy Absorbtion Capability of ZnO Varistors", *IEEE Transactions on Power delivery*, Vol. 14, No. 1, January 1999, pp. 152-162.

[6] W. McDermid, "Detection of Premature Aging of Gapless ZnO Arresters", *Minutes of the Fifty-Fifth Annual International Conrefence on Doble Clients*, 1988, Sec. 9-3.1.

[7] H. Breder and T. Collin, "Supervision of gapless Zinc-Oxide Surge Arresters", *IEE Conference on Lightning and Power Systems*, June 1984, pp. 91-95.

[8] S. Shirakawa et al, "Maintenance of Surge Arrester by Portable Leakage Current Detector", *IEEE Transactions on Power Delivery*, Vol. 3, No. 3, July 1988. pp. 998-1003.

[9] P. Kirby, C.C. Erven and O. Nigol, "Long Term Stability and Energy Discharge Capacity of Metal Oxide Valve Elements", *IEEE Transactions on Power Delivery*, Vol. 3, No. 4 , October 1988 pp. 1656 - 1665

[10] H.R. Philipp, and L.M. Levinson, "Low-Temperature Electrical Studies on Metal-Oxide Varistors - A Clue to Conduction Mechanisms", *Journal of Applied Physics*,Vol. 48, No. 4, 1977.

[11] Hanxin Zhu, "Investigation of On-Site Diagnostic Testing Technique for Metal Oxide Surge Arresters", MSc. Thesis, University of Manitoba, 2000.

[12] Hanxin Zhu and M.R. Raghuveer, "Influence of Representation Model and Voltage Harmonics on Metal Oxide Surge Arresters", *IEEE Transactions on Power Delivery*, Vol. 16, No. 4, October 2001 pp. 599-603.

[13] J. Lundquist, L. Stenstrom, A. Schei and B.Hanson, "New method for Measurement of the Resistive Leakage currents of Metal-Oxide Surge Arresters in Service", *IEEE Transactions on Power Delivery*, Vol. 5, No. 4, November 1990, pp. 1811-1822.

[14] Surge Arrester Monitor application of LCM - Leakage Current Monitor Information LCM-99-001, TransiNor As, January 1999

[15] Christian Heinrich and Volker Hinrichsen, "Diagnostics and Monitoring of Metal Oxide Surge Arresters in High Voltage Networks - Comparison of Existing and Newly Developed procedures", *IEEE Transactions on Power delivery*, Vol.16, No. 1, January 2001, pp. 138-143

[16] Cuijiao Ma, "On-Site Diagnostic Testing of MOSA Using the Neutral Current Method", MSc. Thesis, University of Manitoba, 2003.

[17] Xiangxiao Qiu, "Diagnostic Methods to Detect Ageing in MOSA Valve Elements", MSc. Thesis, University of Manitoba, 1995.

[18] Chandana Karawita, M.R. Raghuveer, "On-Site MOSA Condition Assessment - A New Approach", *IEEE Transactions on Power Delivery*, 2005, Accepted

[19] Chandana Karawita, M.R. Raghuveer, "Leakage Current Based Assessment of Degradation of MOSA Using an Alternative Technique", *IEEE Conference on Electrical Insulation and Dielectric Phenomenon, CEIDP*, Nashville, TN, October 2005. 3 pages, Accepted